Numerical and analytical prediction of pressure and impulse from vented gas explosion in large cylindrical tanks

Jingde Li[1,a], Hong Hao[1,b]

[1]Tianjin University and Curtin University Joint Research Centre of Structural Monitoring and Protection, School of Civil and Mechanical Engineering, Curtin University, Kent St, Bentley WA 6102, Australia

[a]jingde.li@curtin.edu.au, [b]hong.hao@curtin.edu.au

Abstract

This paper presents an extension of previous study on estimating the internal and external pressure and impulse from vented gas explosion in large cylindrical tanks. Unlike the small-medium scale explosion from cylindrical tanks in previous work, explosion pressure and impulse from large-scale explosions are numerically and analytical investigated in this study. CFD simulations are conducted and validated by using experimental data. Sensitivity study on grid selection for large-scale explosion simulations is performed. By adopting two scale-up factors for the analytical correlations, the internal pressure and external pressure on adjacent tanks from vented gas explosion in a tank are accurately predicted. Parametric study of the effectiveness of separation gap between adjacent tanks on pressure and impulse mitigation is also carried out. Influences of the venting size, tank diameter and tank height on the effectiveness of separation distance for pressure and impulse mitigation from large-scale vented gas explosion in an adjacent tank are studied.

Keywords: large-scale gas explosion; vented gas explosion; external pressure; far field; CFD; safe separation gap

1. Introduction

Application of venting is one of the cheapest and simplest ways to mitigate gas explosion despite the complexity of the vent process (Mercx et al., 1992). In order to study the venting process and mechanisms, there have been numerous experimental, numerical and analytical studies (Bradley and Mitcheson, 1978; Ferrara et al., 2006; Russo and Di Benedetto, 2007; Kasmani et al., 2013) on vented gas explosions. Based on a large amount of experimental data and analytical predictions, some correlations (Swift, 1989; Rota et al., 1991; Molkov et al., 2000) have been proposed and adopted in the vented gas explosion design codes (Rodgers and Zalosh, 2013), such as the National Fire Protection Association-68 (NFPA-68).

However, the majority of existing vented gas explosion studies are conducted by using small to medium enclosures. For example, (Ferrara et al., 2008) gained experimental data from a pilot scale (0.2 m^3) cylindrical vessel for the analysis of interaction between internal and external vented gas explosions. The study on the flame propagation and gas explosion in propane/air mixtures done by Liu et al. (Liu et al., 2015) were performed in a 1.16 m^3 explosion chamber. Similarly, in the investigation of temperature and initial enclosure pressure effects on gas explosion by Cammarota et al. (Cammarota et al., 2010), the explosion tests were performed in the cylindrical tank reactor with a diameter of 0.135m and a height of 0.4m.

Although there are some large-scale vented gas explosion experimental studies (Solberg et al., 1981; Harrison and Eyre, 1987; Tomlin et al., 2015), most of the explosion chambers used for experiments were cuboid-shaped chambers. Very limited literatures of vented gas explosion were conducted in large-scale cylindrical tanks. It is pointed out by (Catlin, 1991) that the scale effect on vented gas explosion is not negligible since the turbulence strain rate and chemical time scale ratio in larger scale explosions are different.

Therefore, in order to study large-scale vented gas explosions in cylindrical tanks, it is essential to investigate them in actual scale models. Even though the authors have performed a series of experiments by using 1.5m diameter and 1m height tanks (Li et al., 2017; Li and Hao, 2018; Li et al., 2018), large explosion pressures over 15 kPa were rarely obtained. Especially the external pressures, i.e., pressure recorded outside the explosion tank, from these tests were generally below 2 kPa. For a more meaningful structure safety or structure response study, large pressures from large-scale experiments are expected. However, large-scale experiments are impractical for most labs owing to the cost and safety concerns. Consequently, Computational Fluid Dynamics (CFD) simulations are conducted in this study to investigate larger scale vented gas explosions, existing experimental data are used for numerical data calibration.

In addition to the focus on large-scale vented gas explosion study, effectiveness of separation gap between adjacent tanks on gas explosion pressure and impulse mitigation is another main investigation objective in this study. Firstly, a series of small-medium scale methane-air explosion experiments conducted by the authors with different gas concentrations, vent area sizes and tank combinations are briefly introduced. Secondly, CFD simulations corresponding to all experiments are carried out. The CFD simulation accuracy is validated by comparing the numerical data with experimental data. Sensitivity study of CFD models consisting of a large explosion tank and a large adjacent tank with scaled-up grids is conducted. The empirical relations derived by the authors are applied in this study along with new adjustments for prediction of explosion pressures. Lastly, parametric studies are carried out to investigate the effectiveness of separation distance between adjacent tanks on mitigation of pressures and impulses from large-scale vented explosions in a cylindrical tank.

2. Vented gas explosion experiments and CFD simulation calibration

2.1 Experimental details and CFD simulation setups

A series of vented gas explosions with different methane-air gas concentrations (the concentrations presented in this article are in volume basis), vent opening designs and tank layouts were conducted. The experimental data analyzed in this study and details of equipment parameters can be found in data presented in the authors' previous work (Li et al., 2017; Li and Hao, 2018; Li et al., 2018). Table 1 summarizes the experimental details.

Table 1 Experimental details of different vented gas explosion cases

Case No.	Gas concentration (vol %)	Tank dimension (m)	Sensor location	Vent opening
1	6.5	1.5m diameter, 1m height	On tank wall at 0.75m height	One 130×280 mm^2 panel on roof edge
2	6.5	1.5m diameter, 1m height	On tank wall at 0.75m height	One 305×610 mm^2 panel on roof
3	6.5	1.5m diameter, 1m height	On tank wall at 0.75m height	Two symmetric 305×610 mm^2 panel on roof
4	9.5	1.5m diameter, 1m height	On tank wall at 0.75m height	One 305×610 mm^2 panel on roof
5	9.5	1.5m diameter, 1m height	On tank wall at 0.75m height	Two symmetric 305×610 mm^2 panel on roof
6	12.5	1.5m diameter, 1m height	On tank wall at 0.75m height	One 305×610 mm^2 panel on roof
7	9.5	8 of 1.5 diameter and 1m height tanks in group	On tank wall at 0.75m height	Two symmetric 305×610 mm^2 panel on roof

For explosion cases No. 1 to 6, cylindrical tanks of 1.0m height and 1.5m diameter were designed according to the American Petroleum Institute Standard (API-650, 2007). Tank walls are made of Q345B steel with tensile strength of 0.47 GPa and yield strength of 0.35 GPa (Li and Hao, 2018). The total vent area sizes vary from 0.036 m^2 to 0.37 m^2 in these 6 cases. The methane-air concentrations of 6.5 vol %, 9.5 vol % and 12.5 vol% were tested. One larger-scale vented gas explosion test, namely case No. 7, was also carried out. This gas explosion test consisted of 8 tanks of the same size used in case No. 1 to 6 to study the pressures on the adjacent tanks from vented explosions in the tank located at the center of the tank group.

All tanks' bottom plates are anchored to a reinforced concrete foundation to ensure the tanks stay stationary during the vented explosion testing. High Speed Video Camera (HSVC), Gas

Flow Control System (GFCS) and Piezo-resistive sensors are used. The sensors are installed to record internal pressures in all the cases. A recirculation pump to fill methane into the tank and an infrared methane analyzer to control methane-air concentration are used in the GFCS. The fan and air pump as seen in Fig. 1 are used to continuously fill and mix the flammable atmosphere in the tank. In order to ensure the homogeneity of the gas concentration inside the tank, about 10 to 20 minutes is required to mix the gas mixture. A probe connected to the air pump is inserted into the tank from the gas concentration measuring point as seen in Fig. 1, while the other side of the air pump connected to the infrared gas concentration analyzer provided up-to-date gas concentration data. When the gas concentration inside the tank reached a steady data of 9.5 vol % for 10 minutes as indicated by the infrared methane analyzer, the homogenization of gas mixture for the whole region was deemed achieved.

The ignition sources are electric spark plugs. Centre ignitions are conducted for all tests. Ambient temperature is between 15 degree and 28 degree at the experiment site. To facilitate comparison with the numerical simulation data, all starting times of the raw experimental data are adjusted to zero.

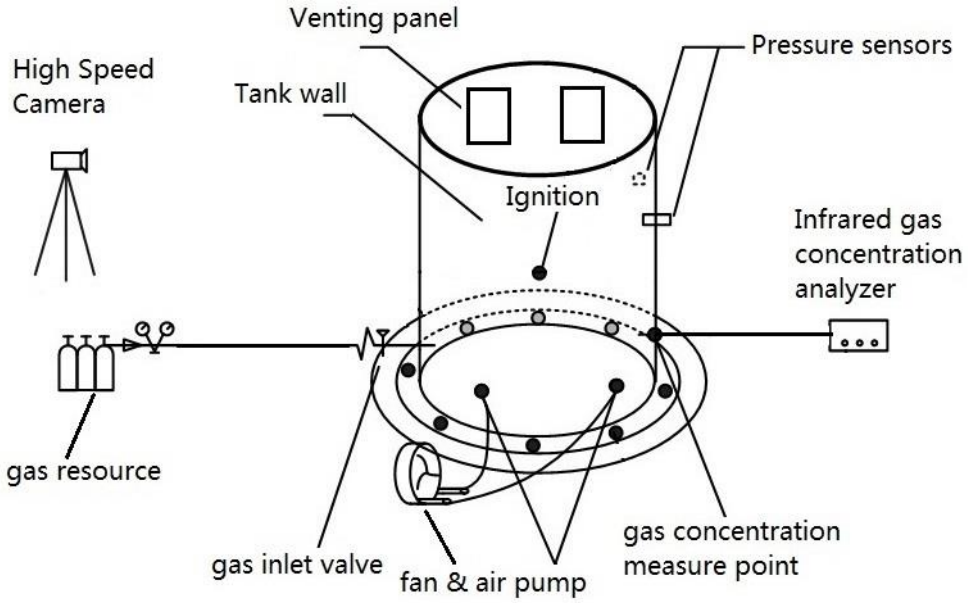

Fig. 1 Gas flow control system scheme (Li and Hao, 2018).

For numerical simulation, a commercial CFD software FLACS v10.7 (Gexcon, 2017), which relies on the Reynolds-Averaged Navier-Stokes (RANS) k-ε model equations, burning velocity data, correlations, energy balance and turbulence equations (Hjertager, 1984, 1993; Arntzen, 1998; Ferrara et al., 2006), is utilized in this study for vented gas explosion simulation. The finite volume method is used in FLACS to solve the compressible Navier-Stokes equations, and the SIMPLE pressure algorithm (Patankar, 1980) is employed for the highly confined explosion simulation. In FLACS, the laminar burning velocity and flame turbulent burning velocity are based on the pre-defined tables and Bray's expression (Bray, 1990). During the vented gas explosion simulation, diffusion is increased by a factor of beta and reaction rate is reduced by a factor of 1/beta, which eventually thickens the flame zone in combustion modelling. The flame thickness is between 3 and 5 grid cells under the selected beta value in FLACS (Vyazmina and Jallais, 2016).

For all simulations, the atmosphere pressure of 1 barg is used as the initial condition, tank roof and wall are modelled as rigid in FLACS. Grid cells are modelled as cubical in the combustion region. The combustion region's volume is specified to be at least 9 times larger than the tank

size. Based on the authors' previous sensitivity studies (Li et al., 2017; Li and Hao, 2018; Li et al., 2018), a grid size of 0.05m within the combustion region is used for small-scale simulation (1.5m diameter and 1m height tank) in this study, while 0.5-1m grid cell is more commonly used for large-scale oil and gas explosion simulation, such as explosion in a fixed offshore platform. Starting from the venting direction, the grid cells are stretched with an increment ratio between 4-10%.

2.2 Different vent opening designs of 6.5 vol % gas concentration case

As seen in Fig. 2 (a) to (c), three different vent openings are designed for the 6.5 vol % methane-air concentration explosion tests. From case No.1 to case No. 3, the vent areas are 0.036 m^2, 0.19 m^2 and 0.37 m^2, respectively. A hinged light-weight steel panel sealed with latex foam, a polyethylene film and two REMBE vent panels with activation pressure of 15 kPa (REMBE, 2015) are used for the aforementioned three cases. The ignition point is located at the center of each tank.

Fig. 3 shows the FLACS 3D geometries of the corresponding experimental cases. 10% meshing increment is used for the grid stretching. 15 grid cells are specified at the smallest vent panel. Eulerian boundary condition is used for these three CFD simulations as in the authors' previous study (Li et al., 2017) that focused on the internal pressure simulation, and since the reflection effect of pressure wave to internal pressure is minimum as the z-direction domain is sufficiently large. Whereas the PLANE_WAVE boundary conditions are generally used in the following large-scale simulations to eliminate pressure wave reflection effect (Hansen et al., 2010; Hansen and Johnson, 2015; Cen et al., 2017). Monitor points are located close to tank's vent panel and on tank's wall at different heights, as seen in Fig. 4. The monitor points at height of 0.75m on tank wall are used to record the internal pressures of vented gas explosions in FLACS. Hinged panels with weight of 1 kN/m^2 are used for model case No. 1 and case No. 3, while the POPOUT relief panel in FLACS is used to model the polyethylene film panel for case No. 2.

The activation pressure for the venting design case No.1 and No. 2 are 6.6 kPa and 1.4 kPa, which are corresponding to the initial vent opening pressure in the experiment Case No. 3 by Li et al., (2017) and the opening pressure in the 6.5 vol % gas concentration experiment by Li and Hao (2018), respectively.

(a) Venting design case No. 1 (b) Venting design case No. 2 (c) Venting design case No. 3

(d) Case No. 1 during explosion (e) Case No. 2 during explosion (f) Case No. 3 during explosion

Fig. 2 6.5 vol % gas concentration experiments for case No.1, No.2 and No. 3

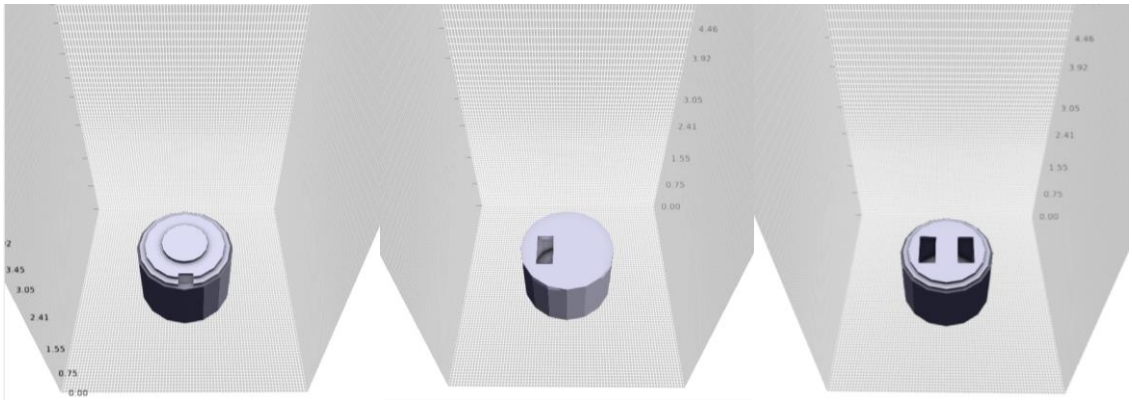

(a) Venting design case No. 1 (b) Venting design case No. 2 (c) Venting design case No. 3

Fig. 3 6.5 vol % gas concentration CFD models for case No.1, No.2 and No. 3

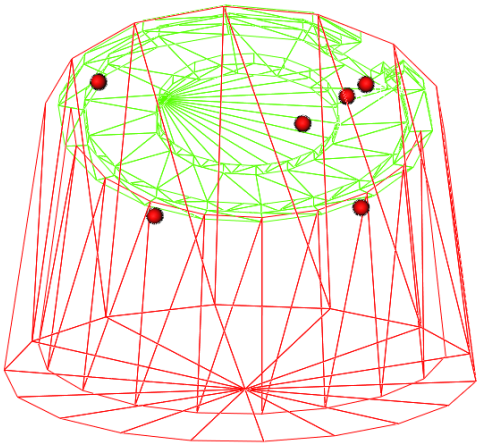

Fig. 4 Locations of monitor points

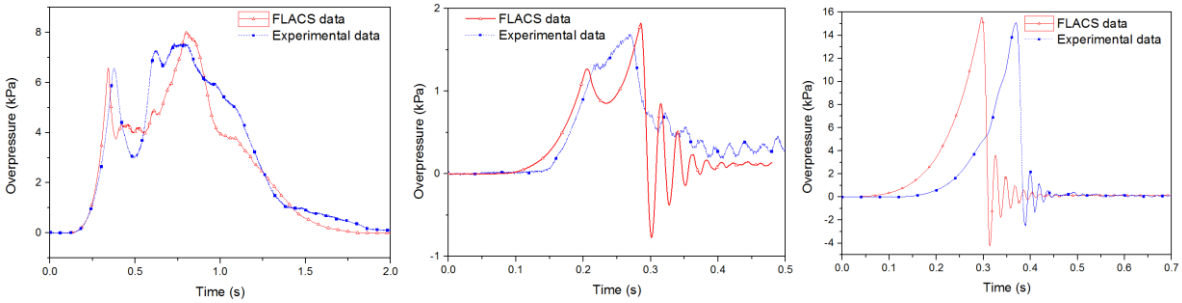

(a) Venting design case No. 1 (b) Venting design case No. 2 (c) Venting design case No. 3

Fig. 5 Comparison of experimental data and FLACS data for 6.5 vol % gas concentration case No.1, No.2 and No. 3

The experimental internal pressure-time histories are compared with FLACS simulation data as shown in Fig. 5. The internal pressures extracted from the monitors in FLACS are at the same locations of the sensors installed in the tests. It can be seen that the internal pressure data predicted by FLACS agree well with the experimental data. The differences in overpressure peaks obtained from FLACS and experiments are less than 10%, although the first peaks appear earlier in numerical simulations than the peaks in the experiments, which is consistent with the observation in other researchers' studies (Pedersen and Middha, 2012; Vyazmina and Jallais, 2016). For small vent area cases No. 1 and No. 2, there are two obvious overpressure peaks while there is only one overpressure peak for case No. 3 with larger vent area. The main reason is that the small vent panel in case No. 1 and case No. 2 results in longer duration of

venting process and more unburned gas is consumed inside the tank. Further flame expansion and pressure growth are developed in these two cases due to the external explosion outside the chamber. When the flame area reaches its highest value during external explosion, the second overpressure peak is generated. Whereas for case No. 3, a larger amount of unburned and burned gases are vented due to the large vent area (2 panels activate at early stage). As more unburned gas is jetted out in case No. 3, less unburned gas is consumed during the combustion. Therefore, the instant reduction of internal pressure is expected when the panels open. Owing to the large vent area, there is no external explosion that contributes to the generation of second overpressure peak in case No. 3.

2.3 Different vent opening designs of 9.5 vol % gas concentration case

The same tank used for 6.5 vol % gas concentration explosion is also used for the 9.5 vol % gas concentration in case No. 4 and case No. 5. Only one vent panel on the left hand side is activated for case No. 4, while the panel on the other side is sealed by welding with a yield strength of 0.45 GPa and tensile strength of 0.53 GPa, as seen in Fig. 6(a). For case No. 5, two vent panels are designed. Plastic films are used as the vent panels. The sensor installations, methane-air gas mixing and gas concentration control system are the same as in the 6.5 vol % vented gas explosion cases.

The tanks in experiments are modelled in 1:1 ratio in FLACS, as seen in Fig. 7. Rigid roof and wall are assumed. Centre ignitions are applied for the both cases. POPOUT activation panels with activation pressure of 0.01 barg in FLACS are used to model the plastic film vent panels installed on the roof. The cuboid boundary region has the x-direction and y-direction dimensions more than 4 times larger than the tank radius. The z-direction is the venting direction, therefore, the z-direction dimension is modelled to be 10 times longer than the tank height. Cubical mesh grids are uniformly distributed inside the combustion region, while other grids are stretched with an increment ratio of 7% towards the venting direction.

(a) Design case No. 4 with one vent panel (b) Design case No. 5 with two vent panels

Fig. 6 9.5 vol % gas concentration experiments for case No.4, No.5

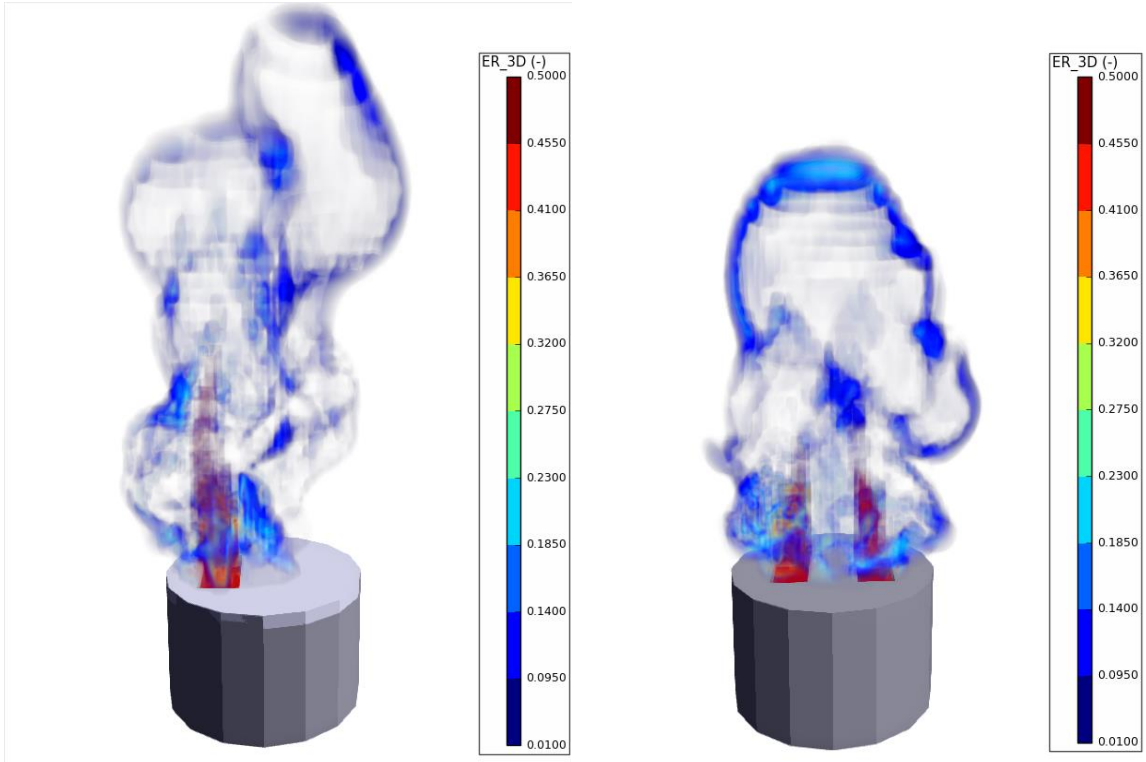

(a) Design case No. 4 with one vent panel (b) Design case No. 5 with two vent panels

Fig. 7 9.5 vol % gas concentration CFD models for case No.4, No.5

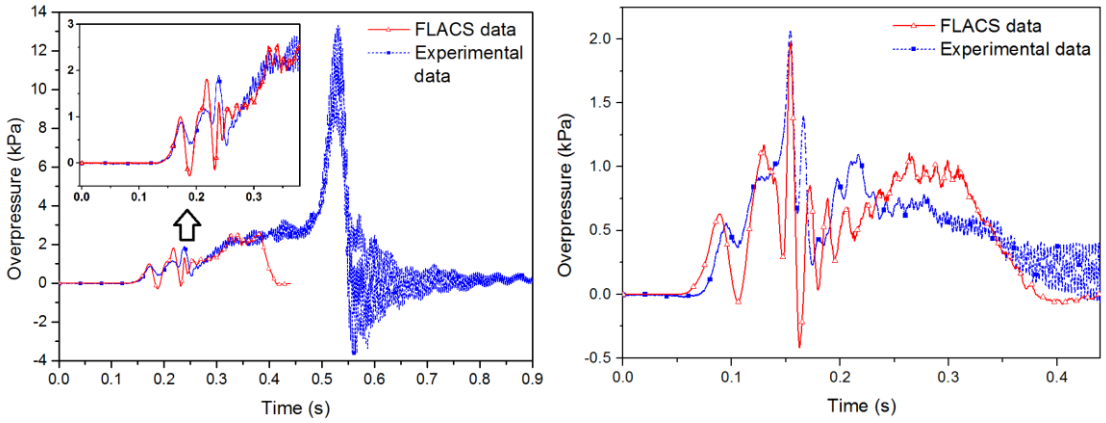

(a) Design case No. 4 with one vent panel **(b) Design case No. 5 with two vent panels**

Fig. 8 Comparison of experimental data and FLACS data for 9.5 vol % gas concentration case No.4, No.5

As seen in Fig. 7, flame developments from vented gas explosion in the both cases are well projected in FLACS 3D view. The comparison of internal pressures from experiments and numerical data in Fig. 8 further verifies the accuracy of FLACS simulation. For the stoichiometric methane concentration of 9.5 vol % case with one vent panel in Fig. 8(a), internal overpressure peaks owing to vent opening and external explosion outside the vent are well predicted by FLACS. In the zoomed-in figure, pressure-time histories due to geometry-induced flame instabilities and turbulence production before 0.4 s are well modelled in FLACS as well. However, due to the fact that the explosion-generated structural vibrations/inductions are not taken into account in FLACS, the overpressure peak (i.e. 13 kPa at 0.52s in Fig. 8(a)) due to flame-acoustic interactions (Bauwens et al., 2010) cannot be reproduced by FLACS (Hisken, 2018). As a matter of fact, so far there is no reliable CFD tool being able to accurately calculate the acoustically driven pressures (Tolias et al., 2018; Vyazmina et al., 2018). Moreover, feedback between acoustics generated by the structure of the chamber and the combustion process is more dominate in front ignition cases of vented gas explosion (Bauwens et al., 2012; Vyazmina and Jallais, 2016). The front ignition explosion study is not within the scope of this article, all experiments and CFD simulations are based on center ignition explosions in this study.

In terms of the two-panel vented gas explosion in Fig. 8(b), the first two peaks due to vent panel opening are accurately predicted by FLACS, although the predicted flame arrival time is slightly earlier. Meanwhile, FLACS simulation data after 0.15s closely resemble overpressure peaks resulted from external explosion and the oscillations due to Rayleigh-Taylor instabilities (Solberg et al., 1981; Tsuruda and Hirano, 1987) in experiments. By comparing the 9.5 vol % cases No. 4 and No.5, it is worth noting that increasing the vent area from one-panel size to two-panel size results in the elimination of acoustically driven overpressure peak.

2.4 One vent opening of 12.5 vol % gas concentration case

Following the above studies on lean combustion of 6.5 vol % concentration case and stoichiometric gas explosion case (i.e. 9.5 vol % methane-air mixture), the vented gas explosion with rich methane-air mixture of 12.5 vol % is also investigated. The same tank and corresponding experimental setups from case NO. 1 to case NO. 5 are used in this section, except the gas concentration is controlled at 12.5 vol %.

Similarly, the FLACS model has 1:1 ratio of the experimental geometry. The panel type, boundary, meshing grid size, aspect ratio of the grid increment, etc. are kept the same as in the previous cases.

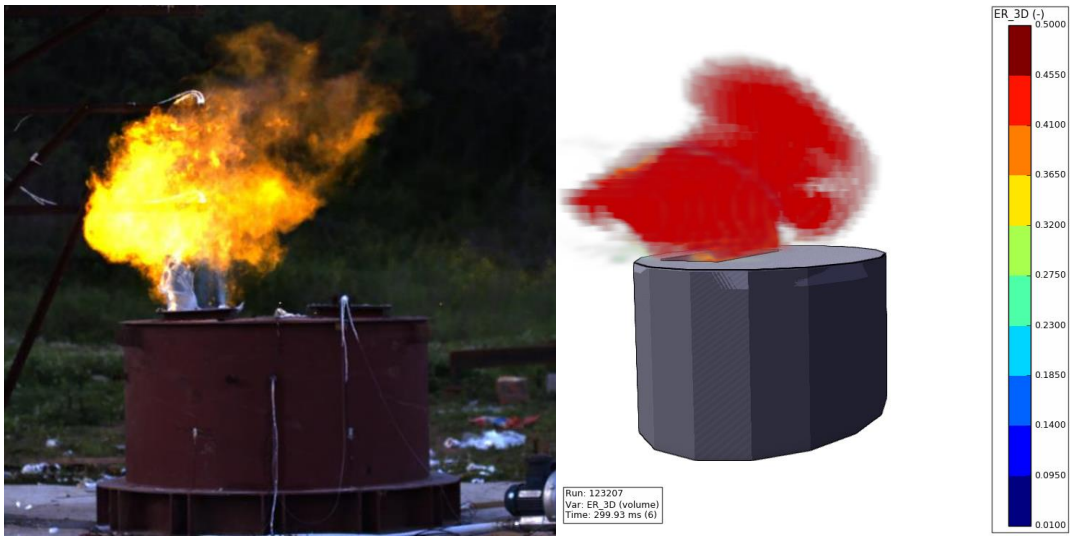

(a)Experiment for case No. 6 **(b) FLACS model for case No. 6**

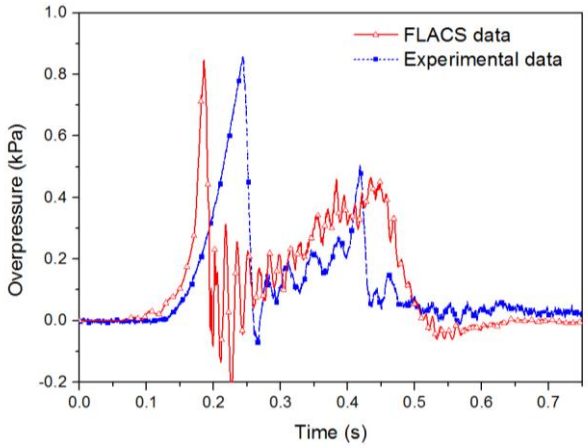

(c) Comparison of experimental data and FLACS data

Fig. 9 Experimental and FLACS data for 12.5 vol % gas concentration case No.6

Compared to the stoichiometric gas explosion in Fig. 6 and Fig. 7, it is interesting to note the combustion of fuel-richer mixture at 12.5 vol % generates more visible red flame as shown in Fig. 9(a) and (b). Despite the fact that the same polyethylene sheets are utilized as the vent panels, it is notable that the first internal overpressure peak (0.85 kPa in Fig. 9(c)) which is related to the vent activation pressure in the 12.5 vol % case is smaller than the first peak (1 kPa) in the one-panel 9.5 vol % case in Fig. 8. Additionally, the rate of pressure rise (pressure increases in the first peak with duration of approximately 0.3s) in 9.5 vol % case is faster than the rate (pressure increases with duration of approximately 0.7s) in the richer fuel mixture case (12.5 vol %). The explanation is that laminar burning velocity at stoichiometric methane concentration of 9.5 vol % is the greatest (i.e. 0.38 m/s) so that the combustion rate reaches the highest (Nishimura et al., 2013). When methane-air mixture concentration increases from 9.5 vol % to 12. 5 vol %, the laminar burning velocity decreases from 0.38 m/s to 0.19 m/s. Slower laminar flame velocity implies lower combustion rate, which eventually results in smaller overpressure peak and lower rate of pressure rise (Bao et al., 2016).

For the 12.5 vol % fuel-rich mixture, FLACS predicted data also agree well with experimental data as shown in Fig. 9(c) in terms of the magnitudes of overpressure peak and combustion duration. However, the first peak calculated by FLACS has a narrower shape and more

oscillations are seen between the first peak and the second peak. Overall, the FLACS predicted internal pressure-time data are reasonable.

2.5 Vented gas explosion in a tank group

From case No. 1 to No. 6, experiments and numerical simulations are conducted based on a single tank with volume of 1.77 m^3. In this section, the experimental and numerical scale increases from a single tank to 8 tanks in a group. As seen in Fig. 10, the tank in the center of the group is confined by an enclosed polyethylene film region with dimensions of 2300×2300×1500 mm^3. 7 enclosed tanks are used to encircle the middle tank and 1 upright truss equipped with water cooling system is placed on one side of the tank group. The separation distance between each two tanks varies from 500 mm to 1000 mm, as shown in Fig. 11. Same experimental facilities and equipment used in case No. 1 to case No. 6 are employed in the tank group testing. Four vales for air inlet, gas inlet, air outlet and gas outlet are equipped for the middle tank. Two fire-resistant fans, a recirculation pump and an infrared methane analyzer are used for gas mixing and gas concentration control.

The center ignition is located inside the middle tank. 9.5 vol % methane-air concentration inside the middle tank and the enclosed film region is used for all tests. The middle tank has no vent covers, which means the vent activation pressure is dependent on the film failure from the cuboid region. Beside the three different separation distances arranged for experiments, all experimental setups are kept the same during explosion tests.

Similarly, the FLACS simulations for three tank group explosions with three different separation distances have the same numerical simulation setups used in the aforementioned cases from No.1 to No. 6. Except the simulation boundaries are extended to cover the whole tank group. The simulation domain has the dimensions of 18000×18000×18000 mm^3.

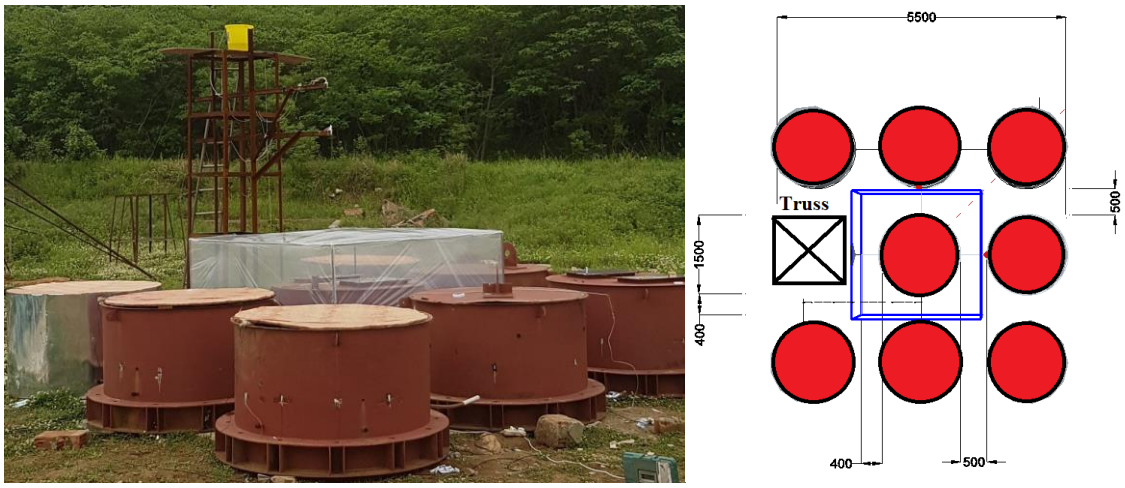

(a) Realistic tank group setup in field (b) Plane graph of the 500m gap example

Fig. 10 Tank group testing setup in experiment

(a) 500mm separation distance (b) 750mm separation distance (c) 1000mm separation distance

Fig. 11 Snapshots of different separation distance cases in experiments

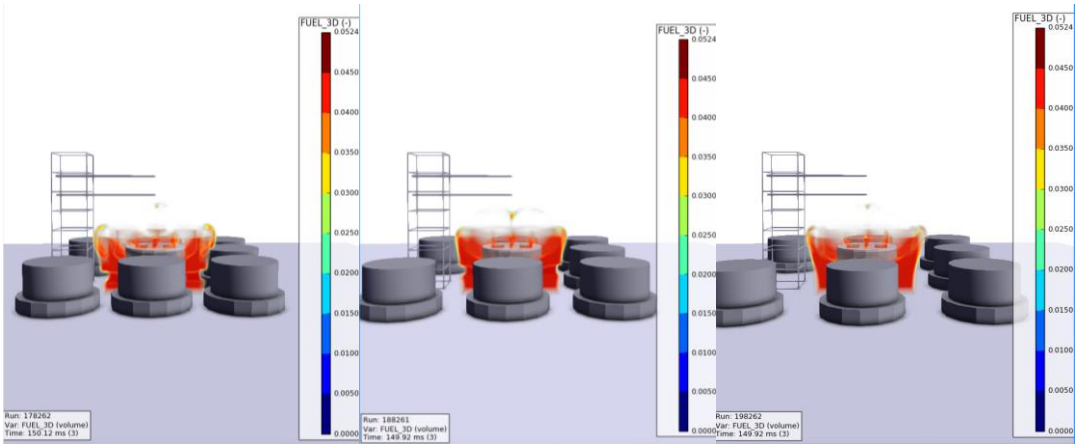

(a) 500mm separation distance (b) 750mm separation distance (c) 1000mm separation distance

Fig. 12 3D models of different separation distance cases in FLACS

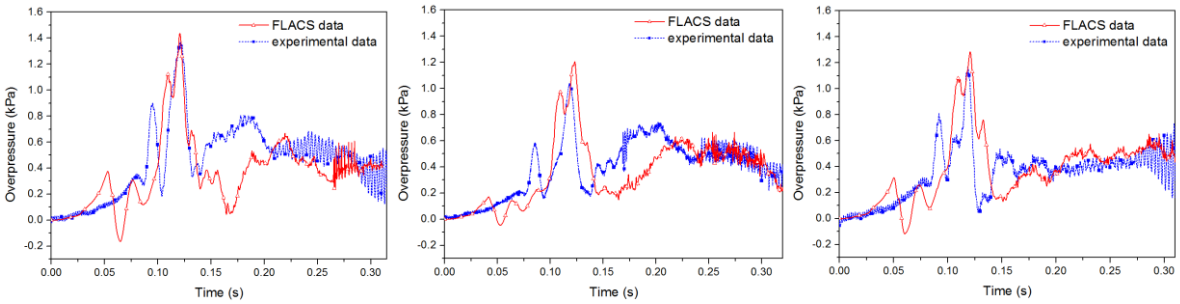

(a) 500mm separation distance (b) 750mm separation distance (c) 1000mm separation distance

Fig. 13 Internal pressure comparison between experimental data and FLACS simulation results

The fuel combustion inside the confined region is well simulated in FLACS as seen in Fig. 12. However, the 0.015mm polyethylene films modelled as light-weight PLASTIC relieve panels in FLACS are invisible. In FLACS, the internal pressure time histories from the 500mm, 750mm and 1000mm separation distance explosion cases are extracted from the monitors inside the center tank. All pressure data are then compared with internal pressures recorded in experiments. The comparison is shown in Fig. 13. In general, the first overpressure peaks and the maximum pressures for all the cases in FLACS agree well with experimental data, although the first peaks from experiments start later than those in FLACS. In all experiments, the Rayleigh-Taylor instability induced pressures after 0.15s as seen in Fig. 13 are well recorded. The correspondingly estimated pressure-time histories in FLACS also satisfactorily demonstrate such instability oscillations. To sum up, for the vented gas explosions with multiple tanks, FLACS provides accurate internal pressure calculation and the predicted pressure development tendencies inside the tank also agree with the experimental data.

3. Large-scale vented gas explosion simulation for large storage tanks

3.1 Grid sensitivity study of large-scale CFD simulation

The aforementioned vented gas explosions from case No. 1 to No. 6 are based on the 1.5m diameter and 1m height tanks (volume = 1.77 m^3). Even though 8 tanks are used in the tank group study with 9 times larger simulation domain size, the grid size still has to be kept as

small as possible so that at least 6-8 grid cells are guaranteed for the vent opening resolution in each tank in FLACS (Gexcon, 2017). Moreover, the maximum overpressure peak calculated by FLACS for cases from No. 1 to No. 6 is 15 kPa.

In this study of large scale vented gas explosions, the tank volumes considered are in the range of 95 m^3 to 308 m^3. Much higher overpressures (higher than 1bar or 100kPa) from such large scale gas explosions are expected. To find the compromise between the simulation accuracy and efficiency for such large-scale vented gas explosion, a new grid sensitivity analysis is conducted to select the suitable grid size. In this study, a cylindrical tank with diameter of 7m and height of 4m (volume of 154 m^3, which is in the middle of the tank volume range) is chosen for the sensitivity study, as seen in Fig. 14.

Both the internal pressures and external pressures between two tanks are calculated in this section. Monitors inside the pressure donor tank on the left hand side and monitors on the wall of pressure acceptor tank on the right hand side as seen in Fig. 14 are set to record the pressures. The pressure donor tank is filled with 9.5 vol % stoichiometric methane-air mixture. Ignition is at the center of the donor tank. Vent opening (600x1000 mm^2) is on the top of the donor tank's side wall facing the pressure acceptor tank. Vent activation pressure is assumed as zero. The acceptor tank has the same dimensions of the donor tank, the separation distance between the two tanks is kept as 1m in the sensitivity study. CFLC = 5 and CFLV = 0.5 for simulations within the explosion region are used. Since the external pressures outside the donor tank are of interest, the time step condition STEP "KEEP_LOW" is applied to reduce smearing of the pressure waves (Hansen and Johnson, 2015). The simulation domain has dimensions of 45000×18000×15400 mm^3.

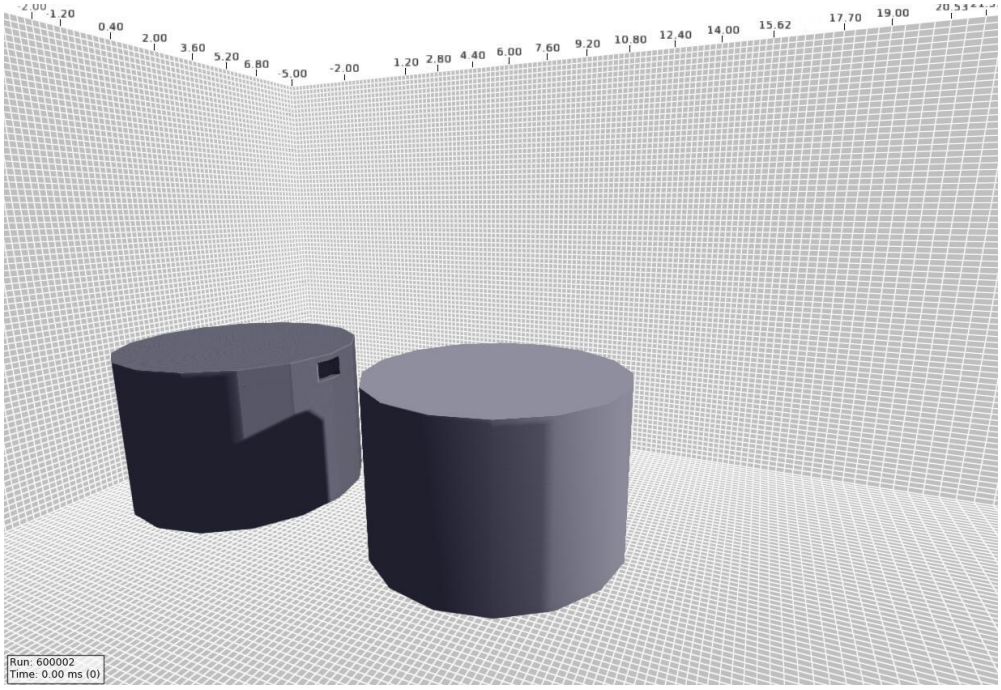

Fig. 14 3D model of 7m diameter and 4m height tanks in FLACS simulation

According to FLACS user guide, the grid resolution should be chosen to obtain an adequately accurate simulation result within an acceptable time frame, which is about a few hours or at least overnight for an explosion simulation. It is not suggested to start a CFD simulation on a grid that will be running for days (Gexcon, 2017). For the 7m diameter and 4m height tank, the grid size of 0.1m results in explosion calculation running for more than 2 days. Therefore, the grid size starting from 0.15m is chosen for the sensitivity study. As seen in Table 2, 5 different grid sizes in the range of 0.15 mm to 0.25 mm are selected for CFD simulation.

Table 2 Sensitivity study details of selected grid size, predicted internal pressure and comparison of pressures between two different grid size cases

Grid size (m)	0.15	0.18	0.2	0.22	0.25
Peak internal pressure (kPa)	237.9	243.4	250.5	255.7	260.5
Difference between neighboring data (%)	-	2.26%	2.83%	2.03%	1.84%
Computational time for 8-core computer	28 hrs	16 hrs	12 hrs	8.5 hrs	6 hrs

Fig. 15 shows the 3D model of flame development during the vented gas explosion. For demonstration purpose, the fuel mass fraction is set between 0.003 and 0.01 in the figure. The time is set at 600ms (i.e. at the early stage of simulation). The cylindrical gas cloud inside the donor tank is ignited at the center of the tank, the unburned and burned gases are jetted out of

the tank from the 600x1000 mm^2 vent opening. The internal overpressure-time history data are extracted from all simulations and shown in Fig. 16. Internal pressures are obtained from the same monitors located on the wall at the same height of 1m inside the pressure donor tank. Since the overpressures inside the tank are homogeneously distributed, only the monitor point located at the height of 1m is used to record the maximum explosion overpressures.

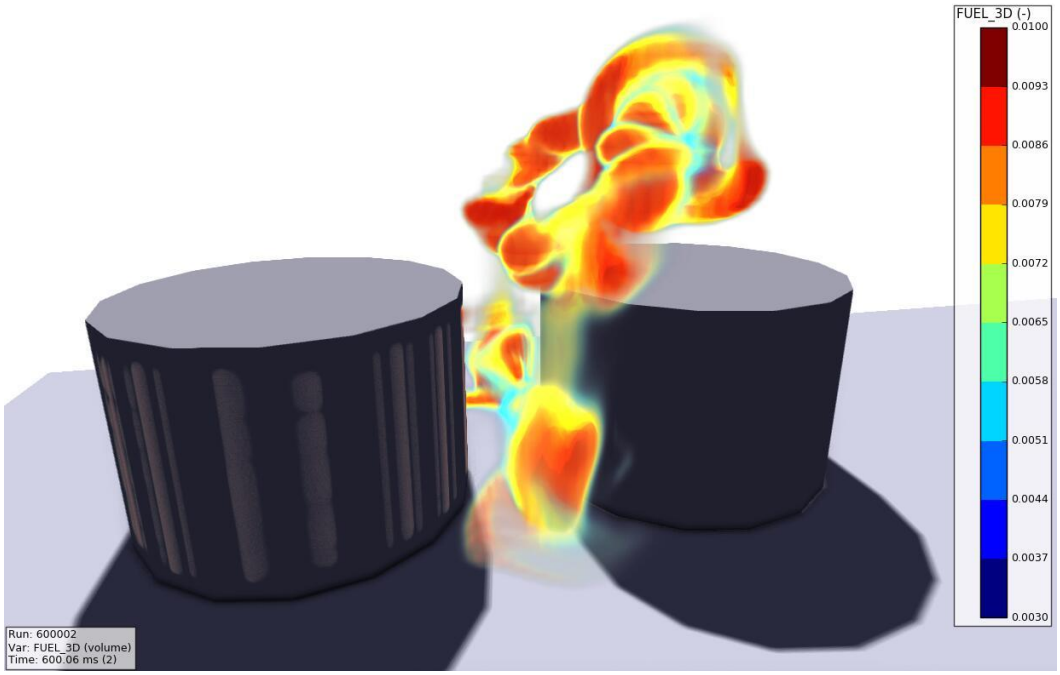

Fig. 15 Flame development of the vented gas explosion from the donor tank in FLACS

In the comparison of Fig. 16, the highest overpressure peak is 260.5 kPa by using 0.25 m grid, the lowest overpressure peak is 237.9 kPa by using 0.15 m grid. From 0.15 m grid to 0.25 m grid, the overpressure peak increases marginally. The pressure difference between each two neighboring cases is below 3%. The maximum difference between the most far-end cases (i.e. the 0.15 m grid case and the 0.25m grid case) is 8.7%, which is deemed acceptable. Therefore it can be concluded that the grid sensitivity in the range of 0.15 m to 0.25 m is convergent. However, the CFD calculation time can increase up to 300 % when the grid size decreases from 0.25 m to 0. 15 m. In order to improve the computational efficiency and to ensure minimum 15 grid cells available at vent opening, grid size of 0.2 m is chosen for all large-scale vented gas explosion simulations in this study.

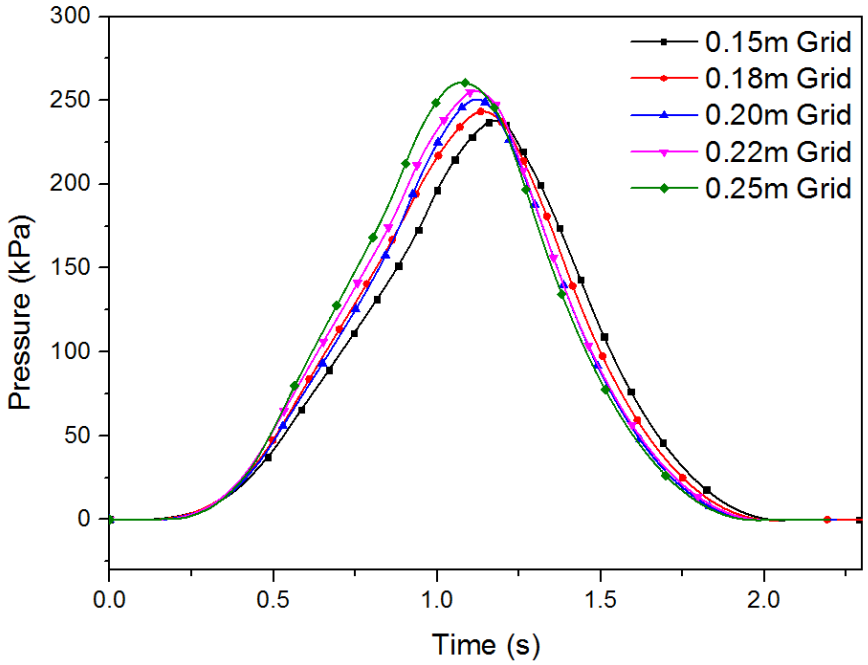

Fig. 16 Comparison of internal pressures from different grid size simulations

3.2 Analysis of internal pressures from vented explosion with different tank volumes by using VMEOC correlations

Having decided the grid cell size of 0.2m, the internal pressures of tanks with volume sizes in the range of 95 m^3 to 308 m^3 are calculated. Specifically, the variable in tank volume is the diameter, which increases from 5.5m to 8.0m in the CFD simulation. While the tank height is kept at 4m and the vent opening size of 600x1000 mm^2 is also unchanged. Vent activation pressure is zero.

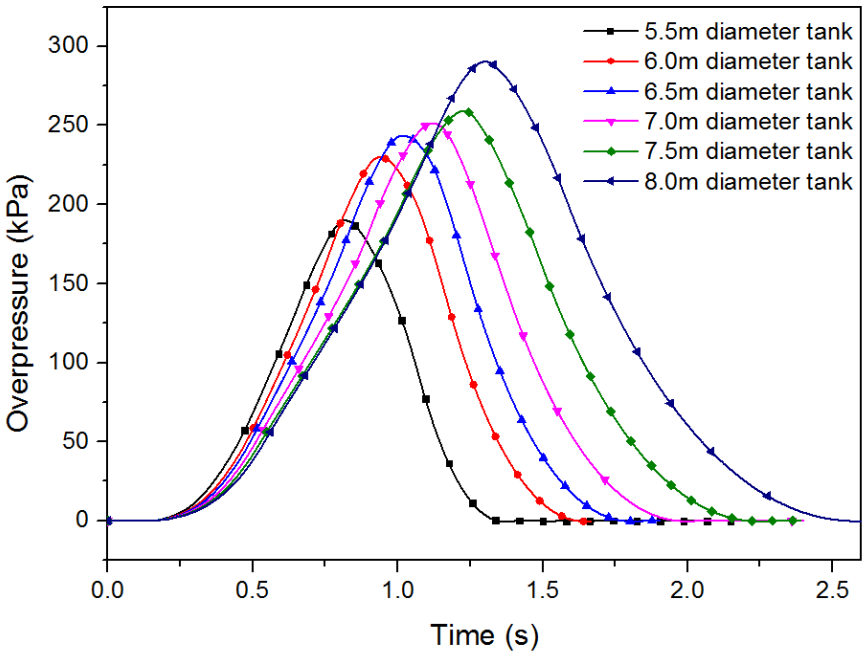

Fig. 17 Internal pressures recorded inside the donor tanks for different tank diameter cases

As seen in Fig. 17, the internal overpressure peak increases proportionally with the tank diameter, as well as the duration of the explosion pressure time history. Therefore, the impulse, which is the integral of the overpressure over time, increases even more significantly than the overpressure peak. This is because the larger tank diameter has larger gas cloud inside the tank. Since the tank volume/dimeter is the only variable, the larger gas cloud will generate more combustion energy once the cloud is ignited, thereby increasing both the pressure and impulse inside the tank.

In the authors' previous study (Li et al., 2017), a series of simplified correlations named Vented Methane-air Explosion Overpressure Calculation (VMEOC) correlations were proposed to predict the internal pressure from vented gas explosion under tank size of 50m^3. In this section, the VMEOC correlations are used to predict the internal pressures from the above 5 larger-scale vented gas explosions. Additionally, another two explosion cases with different vent areas are included as seen in Table 3.

Table 3 Parameter details of different tanks used in the internal pressure analysis by using VMEOC correlations

Explosion No.	Tank diameter (m)	Vent area (m^2)	Tank roof area (m^2)	Ratio[#] of $A_{vo}\times D/(A_{rf}\times H)$
1	5.5	0.6	23.8	0.034
2	6	0.6	28.3	0.032
3	6.5	0.6	33.2	0.029
4	7	0.6	38.5	0.027
5	7.5	0.6	44.2	0.025
6	8	0.6	50.3	0.024
7	7	0.8	38.5	0.036
8	7	1.0	38.5	0.045

[#] The parameters of A_{vo} , D, A_{rf} , H represent the vent area, diameter of tank, roof area and tank height/depth for the ratio used in the vent activation effect calculation.

Table 3 summarizes the parameter details for these 8 explosion cases. In VMEOC correlations, depending on the ratio related to the vent area, tank roof area and tank volume, the internal overpressure peak is calculated as (pressure activation is equal to zero in FLACS simulation):

i. Enclosure with small vent area ratio ($(A_{vo}/A_{rf})\cdot V^{1/3} \le 0.08$)

$$P_{\max} = 1.613\cdot \ln\left[\left(\varphi_{\text{gas}}^{*\left|1-\ln\varphi_{\text{gas}}\right|} - 2.1\left|1-\varphi_{\text{gas}}\right|\right)P_{act}^{*}A_{vo}^{*} + 4\right] \text{-} 1.93 \qquad (1)$$

ii. Enclosure with large vent area ratio ($(A_{vo}/A_{rf})\cdot V^{1/3} > 0.08$)

$$P_{\max} = 1.613\cdot \ln\left[\left(\varphi_{\text{gas}}^{*\left|1-\ln\varphi_{\text{gas}}\right|} - 2.1\left|1-\varphi_{\text{gas}}\right|\right)\cdot\left(3\cdot P_{act}^{*\ 0.3} - 1.7P_{atm}\right)A_{vo}^{*} + 4\right] \text{-} 1.93 \qquad (2)$$

where $P_{\max}$ is the internal overpressure peak, ϕ_{gas}^{*} is the effective gas equivalence ratio, P_{act}^{*} is the effective vent activation pressure, A_{vo}^{*} is the effective vent area ratio, and P_{atm} is the atmosphere pressure.

In order to decide which equation to use, the ratio of γ_{vent} is calculated as:

$$\gamma_{vent} = \frac{A_{vo}}{A_{rf}}\cdot V^{1/3} \qquad (3)$$

where γ_{vent} is the vent area to tank roof area and tank volume ratio, A_{vo} is the vent area, A_{rf} is the roof area, V is the tank volume.

In Table 3, the ratios of γ_{vent} are all over 0.08 except explosion No. 5 and No. 6. Therefore, equation (1) is used for explosion No. 5 and No. 6, while equation (2) is used for other explosion cases.

In equation (1) and equation (2), the effective gas equivalence ratio of ϕ^*_{gas} is calculated as:

$$\phi^*_{gas} = 3.5\ln\left(-4\left|\ln\left(\phi_{gas}-0.1\right)\right|^{\left(\frac{1}{\phi_{gas}+0.1}\right)^{0.7}} - \left|-1+\phi_{gas}\right|+6\right) + \frac{16.80\left(\frac{P_{act}}{P_o}\right)^{0.75}}{V} - 4.1 \quad (4)$$

where ϕ_{gas} is the equivalence ratio of gas, P_{act} is the vent activation pressure, and P_o is the initial pressure (e.g. atmosphere pressure) inside the enclosure prior to ignition.

The effective vent area ratio of A^*_{vo} is calculated as:

$$A^*_{vo} = 4.5\left(0.03530 + 0.01765\left(\frac{1}{1.2}\frac{H}{\mathrm{D}}-1\right)^2\right)\mathrm{D}^{1.82}A_{vo}^{\left(-\frac{2\,\mathrm{D}}{H}\right)} - 0.65 \quad (5)$$

The effective vent activation pressure of P^*_{act} is determined by:

If $\frac{A_{vo}\mathrm{D}}{A_{rf}H} > 0.04$,

$$P^*_{act} = 2.52\ln\left(1+P_{act}^{1.4}\sqrt{\frac{A_{vo}\mathrm{D}}{A_{rf}H}}\right) + 1.26\,P_o\ln\left(\frac{0.02\,V}{A_{vo}}\right) + 2 \quad (6)$$

If $\frac{A_{vo}\mathrm{D}}{A_{rf}H} \le 0.04$,

$$P^{*}_{act} = 0.45\,P_{act} + 1.26\,P_o \ln\left(\frac{0.02\,V}{A_{vo}}\right) + 2 \quad (7)$$

In Table 3, only explosion case No. 8 has the ratio of $A_{vo}\times D/(A_{rf}\times H)$ larger than 0.04, while others are lower than 0.04. The equations (6) and (7) are used accordingly.

By substituting all parameters calculated from equation (3) to equation (7) into equation (1) and equation (2), internal overpressure peaks of Pmax are calculated and compared with FLACS estimated results as shown in Table 4.

Table 4 VMEOC correlations calculated overpressure peaks and FLACS predicted overpressure peaks for explosion cases in Table 3

Explosion No.	VMEOC correlations calculated pressure (kPa)	FLACS predicted pressure (kPa)	Difference between VMEOC and FLACS data
1	509.4	190.5	268.10%
2	562.9	230.4	244.75%
3	613.7	244.3	251.52%
4	662.1	251.6	263.80%
5	767.3	260.4	295.13%
6	815.2	290.1	281.11%
7	493.6	169.3	292.07%
8	363.9	112.4	324.96%

It is seen in Table 4 that VMEOC correlations estimated overpressure peaks are about 3 times the overpressure peaks of FLACS. The 3 times difference between two sets of data is mainly due to the simulation scale difference. It is worth pointing out that the current CFD models are in large-scale, while the correlations derived earlier were based on small-medium scale tanks. The secondary reason is the grid cell size difference between the numerical models used in VMEOC correlation development and the numerical models in the current simulation. In authors' previous study on VMEOC correlations, all CFD simulations (over 350 cases) were conducted based on 0.05 m grid size, while the grid size in current cases are 0.2m. As seen in section 3.1, from grid size 0.18 m to 0.2 m, the overpressure peak difference is 2.83%. The pressure difference can be even larger if the grid size increases from 0.05 m to 0.2 m. The previously derived VMEOC can be used to predict overpressure for a tank with volume up to

467 50m^3. However, for case No.6 with 154m^3 tank in Table 4, the pressure predicted by the original
468 VMEOC is 815.2 kPa, which is even larger than the highest pressure (i.e. 750 kPa) from an
469 idealized vented explosion (i.e. explosion from a nearly fully-closed vessel) with 9.5 vol %
470 methane-air mixture (NFPA-68, 2007). In other words, the previously derived VMEOC
471 overestimates pressure for vented gas explosion from a tank with size over 50m^3. Therefore, in
472 this study, a factor of α is required to adjust the VMEOC correlations for large-scale vented
473 gas explosion. However, owing to the cost and safety concerns for large-scale experiments,
474 only CFD simulations are conducted in current study. The sensitivity study in section 3.1
475 assures large-scale simulation results' convergence and accuracy. α equals to 0.35 is
476 determined in this study based on all large-scale CFD simulation data. As a guidance in this
477 study, the factor of α is only used as a reference factor, which may vary depending on the
478 simulation scale and grid size selection.

479 For vented gas explosion with zero vent activation pressure in different simulation domain
480 scale, the adjusted VMEOC correlations are expressed as:

481 **iii. Enclosure with small vent area ratio ($(A_{vo}/A_{rf})\cdot V^{1/3} \le 0.08$)**

482 $$P_{\max} = \alpha\left\{1.613\cdot\ln\left[\left(\varphi_{\text{gas}}^{*\left|1-\ln\varphi_{\text{gas}}\right|} - 2.1\left|1-\varphi_{\text{gas}}\right|\right)P_{act}^{*}A_{vo}^{*} + 4\right] - 1.93\right\} \quad (8)$$

483 **iv. Enclosure with large vent area ratio ($(A_{vo}/A_{rf})\cdot V^{1/3} > 0.08$)**

484 $$P_{\max} = \alpha\left\{1.613\cdot\ln\left[\left(\varphi_{\text{gas}}^{*\left|1-\ln\varphi_{\text{gas}}\right|} - 2.1\left|1-\varphi_{\text{gas}}\right|\right)\cdot\left(3\cdot P_{act}^{*\,0.3} - 1.7P_{atm}\right)A_{vo}^{*} + 4\right] - 1.93\right\} \quad (9)$$

485 By using the correction factor of $\alpha = 0.35$, the adjusted VMEOC correlations predicted
486 overpressure peaks are updated and compared with FLACS calculated results, as shown in Fig.
487 18. It is noted that the R-square value between two sets of data is 0.89, which means the newly
488 adjusted VMEOC correlations can predict internal pressures with 89% accuracy for these large-
489 scale vented gas explosions.

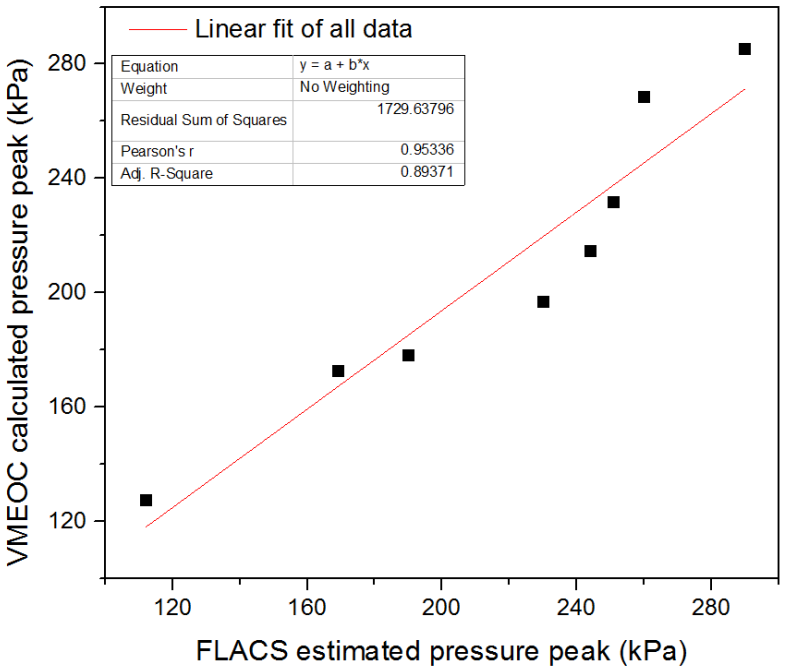

Fig. 18 Comparison of FLACS estimated internal overpressure peak and VMEOC calculated data

3.3 Analysis of external pressures from vented explosion with different tank volumes by using dimensionless correlations

In the comparison of internal pressures from different donor tanks in the above section, the explosion pressure from the vented gas explosion can be over 2 barg (i.e. 200 kPa), which may generate supersonic flow velocity if detonation occurs. It is defined that gas explosion includes two scenarios, i.e., deflagration and detonation. For deflagration, the flame propagates with subsonic velocity in the range of 1-1000 m/s. While the detonation wave has flame velocity over 1500 m/s (Bjerketvedt et al., 1997; Pasman, 2015).

For vented gas explosion in the aforementioned cases in Table 3 and Table 4 , the flame velocity in external explosion is highly likely to reach sonic speed (i.e. 343 m/s). Therefore, the correct selection of flame development criterion in FLACS is important, especially when the external pressures are the study focus in this section. Taking the tank of explosion No. 1 and No. 5 in Table 3 as examples, the tank in case No. 1 has the smallest diameter of 5.5m among all the considered cases, the tank in case No. 5 has a relatively large diameter of 7.5m. The flame

508 velocities at 0.9s and 1.2s generated from the donor tank (tank filled with gas cloud) for two
509 cases are shown in Fig. 19. It is clearly seen that the flame speed from the vent in case No. 1
510 can propagate at a speed over 1000 m/s, which is beyond the deflagration sonic velocity upper
511 limit. Meanwhile, the flame speed in case No. 5 reaches the lower limit of supersonic flame
512 speed of 1500 m/s.

513 In order to accurately model turbulence and flame development between two tanks with a
514 separation gap, in the SETUP file, a keyword of KEYS="PS1=01" is used as a criterion in
515 FLACS to ensure the maximum speed exceeding the sonic speed during combustion is taken
516 into account.

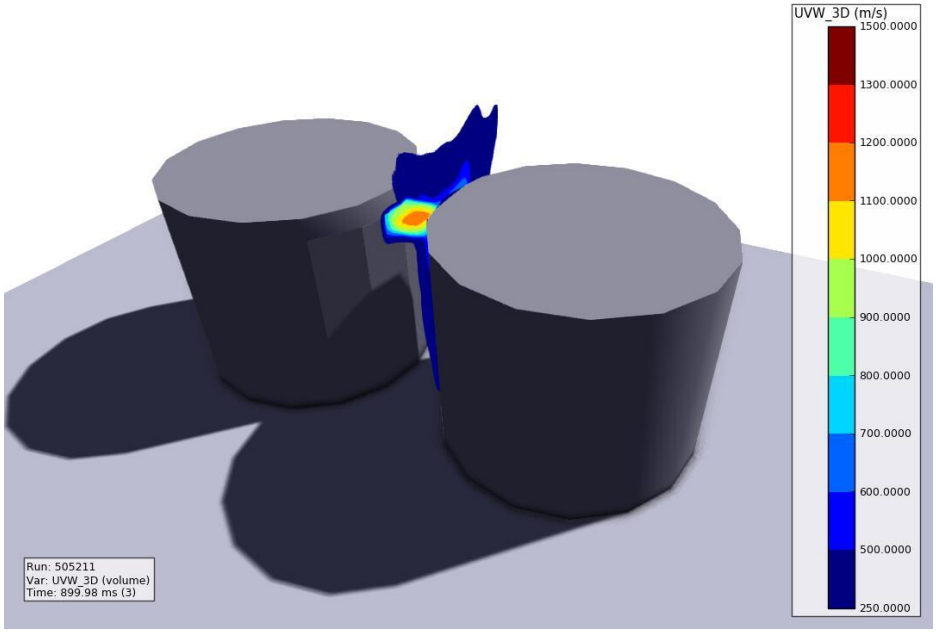

517
518 **(a) 5.5 diameter tank of explosion No. 1 in Table 3**

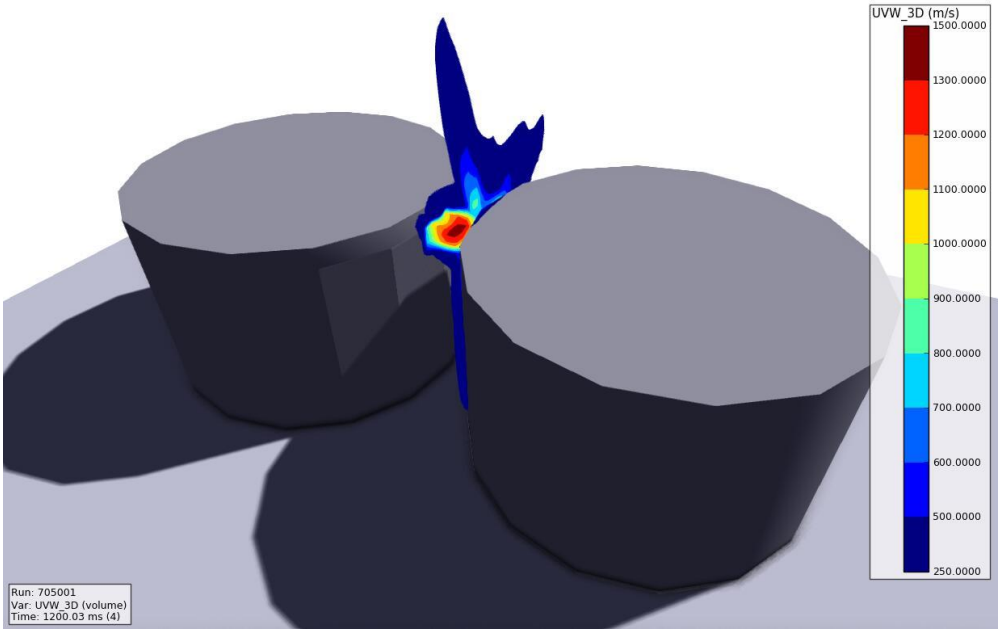

(b) 7.5 diameter tank of explosion No. 5 in Table 3

Fig. 19 3D view of flow velocity at 0.9s and 1.2s for two different vented gas explosions

In FLACS, external pressures are recorded by the external monitor on the pressure-accepting tank wall. The external monitor is allocated directly opposite the vent as seen in Fig. 20. In addition to the monitor on the pressure-accepting tank, a passive panel to record the averaged external pressures is also used. The passive panel in FLACS is an inactive panel that does not affect the numerical simulation in any respect but records variables (e.g. pressure data). The area size of the passive panel is set to 0.6 m^2 to get the averaged pressure. The location of the panel is fixed in the simulations in this study for investigation of pressure decay and the subsequent parametric simulations of the separation distance effect on pressure mitigation. As shown in Fig. 20, the pressure-time data starting from the vent is also recorded by the vent-pressure monitor located in the middle of the vent. The vent-pressure monitor and external-pressure monitor are on the same axis perpendicular to the vent.

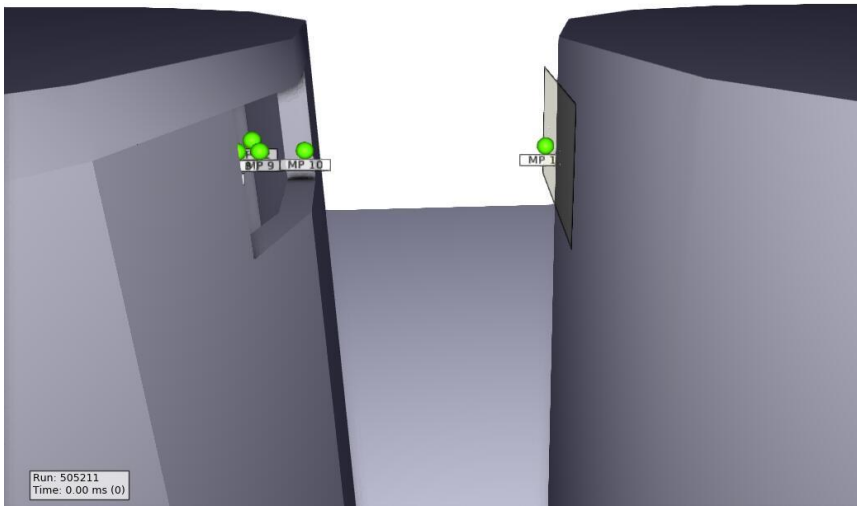

Fig. 20 3D view of monitors near the vent of the donor tank and data recording panel on the acceptor tank in FLACS simulation

Although a new approach by (Hansen et al., 2010; Hansen and Johnson, 2015) has been proposed to improve the far-field pressure prediction accuracy of FLACS, overpressures predicted by FLACS in the far field may still decay too quickly. Especially if the external pressures are recorded at a far distance more than twice of the tank diameter and when the CFLC and CFLV parameters are not small enough (e.g. CFLC = 5 and CFLV = 0.5). Due to such simulation limitation and high computational cost (if CFLC and CFLV are decreased further) in FLACS, the distance between two tanks chosen in this study is decided to vary in a small range of 1m to 3m. In practice, if separation distance is more than 3 m, the pressure on the adjacent tank is expected to be smaller than that when the separation distance is 3 m.

The external pressure decay between two tanks is then investigated by conducting FLACS simulation and the results are compared with the far-field pressures estimated by using the dimensionless correlations from the authors' previous study (Li and Hao, 2018). The explosion No. 2, No. 4 and No. 6, which are tanks with diameters of 6m, 7m and 8m (tank height is 4m as a constant value) are chosen for the external pressure study.

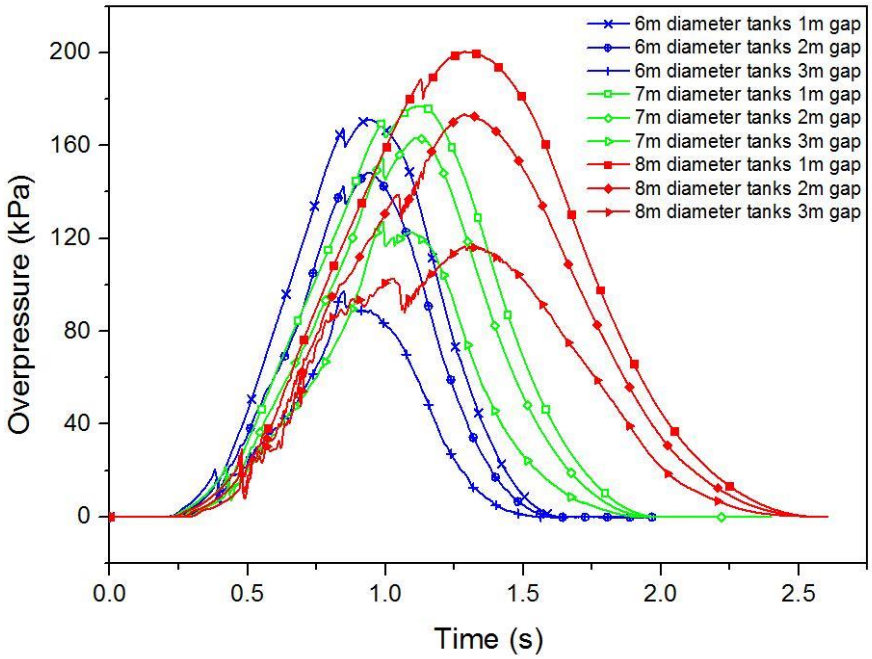

552
553 **Fig. 21 External pressure-time data recorded by external monitors on pressure-accepting tanks**
554

555 In FLACS, the external pressures in 9 cases (i.e. 3 different tank volumes and 3 different
556 separation distances) are recorded by the external monitors on the pressure-accepting tanks as
557 shown in Fig. 21. It is apparent to see larger tank cases has greater overpressure peaks and
558 longer durations of the pressure-time histories. By increasing the separation distance, the
559 overpressure peaks decrease, which is due to the turbulence interruption within the separation
560 gap, as well as geometric attenuation of explosion wave.

561 Overpressure peaks from FLACS in Fig. 21 are extracted and summarized in Table 5 along
562 with tanks' geometry details. The external pressure data are used for the investigation of
563 pressure decay by using the correlations for external pressure calculation.

564 **Table 5 External pressure data and tank geometry details for pressure decay calculation**

Tank diameter (m)	Separation (m)	Tank volume (m^3)	Pressure near vent (kPa)	Pressure on external monitor* (kPa)
6.0	1.0	113.1	102.1	171.2
6.0	2.0	113.1	100.4	148.4
6.0	3.0	113.1	97.4	97.6
7.0	1.0	153.9	108.4	177.2
7.0	2.0	153.9	107.1	163.3
7.0	3.0	153.9	105.5	122.3

8.0	1.0	201.1	114.2	200.4
8.0	2.0	201.1	111.9	172.2
8.0	3.0	201.1	108.8	118.6

565 *The pressures from external monitors on tank wall are reflected pressures.

566 The initial mechanical energy from the vent is calculated by:

567 $$E_g = \frac{\Delta p_v (V - mb)}{\gamma - 1} \quad (10)$$

568 where b is a co-volume constant, which is 0.04278 L/mol, or 0.002674 m^3/kg for methane gas,
569 V and m are the volume and mass of gas inside the tank. The ratio of specific heat γ is 1.32
570 for methane at 20 degrees Celsius. Δp is the overpressure near vent.

571 The explosion energy from the vent is then used to calculate the overpressure in far field with
572 a distance of R in the dimensionless equation as shown below:

573 $$\frac{\Delta P_e}{P_o} = 1.1 \cdot \frac{\Delta p_v}{P_o} \cdot e^{-\left(0.011 \cdot \frac{\Delta p_v}{P_o} + 0.4\right) \cdot \frac{R}{\left(\alpha \cdot E_g / P_o\right)^{1/3}}} \quad (11)$$

574 where ΔP_e is the external overpressure peak, P_o is the ambient atmospheric pressure, α is the
575 mechanical energy coefficient (Molkov and Kashkarov, 2015). For the vented explosion from
576 the side wall, it is assumed there is no reflection of blast wave from the fully-opened vent.
577 Therefore, α=1.0 is used in this study. R is the distance from the vent opening to the pressure
578 monitor point in meters.

579 By using Equation (10) and (11), initial mechanical energies from the vent and external
580 overpressure peaks are determined and given in Table 6. It is worth noting that the overpressure
581 peaks predicted by FLACS in Table 5 are about twice of the analytically calculated
582 overpressure peaks. The difference between these two sets of data is because the dimensionless
583 correlations by the authors were derived based on the single tank experiments, and the pressure

584 decaying were obtained in open space, i.e., not the reflected pressure. Whereas in this study,
585 twin tanks are used in the numerical simulation, simulations are conducted within the region
586 where blast wave propagates from the pressure donor tank to the pressure acceptor tank.
587 Pressure wave is reflected from the wall of pressure-accepting tank.

588 **Table 6 Calculation of mechanical energy and external overpressure peak by correlations in**
589 **different cases**

Tank condition	Mechanical energy (MJ)	Correlation-calculated pressure (kPa)	Different between correlation-calculated data and FLACS estimated data
6m diameter tanks with 1m gap	36.1	90.6	188.9%
6m diameter tanks with 2m gap	35.5	72.1	205.8%
6m diameter tanks with 3m gap	34.4	56.9	171.5%
7m diameter tanks with 1m gap	52.1	97.8	181.2%
7m diameter tanks with 2m gap	51.5	79.4	205.8%
7m diameter tanks with 3m gap	50.7	64.4	189.9%
8m diameter tanks with 1m gap	71.7	104.3	192.1%
8m diameter tanks with 2m gap	70.3	85.2	202.1%
8m diameter tanks with 3m gap	68.3	69.4	171.0%

590
591 Despite the reflection factor (in the range of 1.7 to 2.1), the pressure decaying trend simulated
592 by FLACS in large-scale tanks agrees well with the pressure decreasing trend estimated by
593 correlations, as seen in Fig. 22. By increasing the separation distance from 1m to 3m, the
594 overpressure peaks proportionally decrease. In the comparison of two sets of data from 9
595 different cases, the R-square values are between 89% and 94.7%. Therefore, it can be
596 concluded that the correlations used for far-field/external pressure calculation by (Li and Hao,
597 2018) can accurately predict the external pressure decay between two large tanks. However, an
598 appropriate pressure reflection factor (1.7 to 2.1 in this study) should be used for the calculation
599 of external pressure reflected from tank wall.

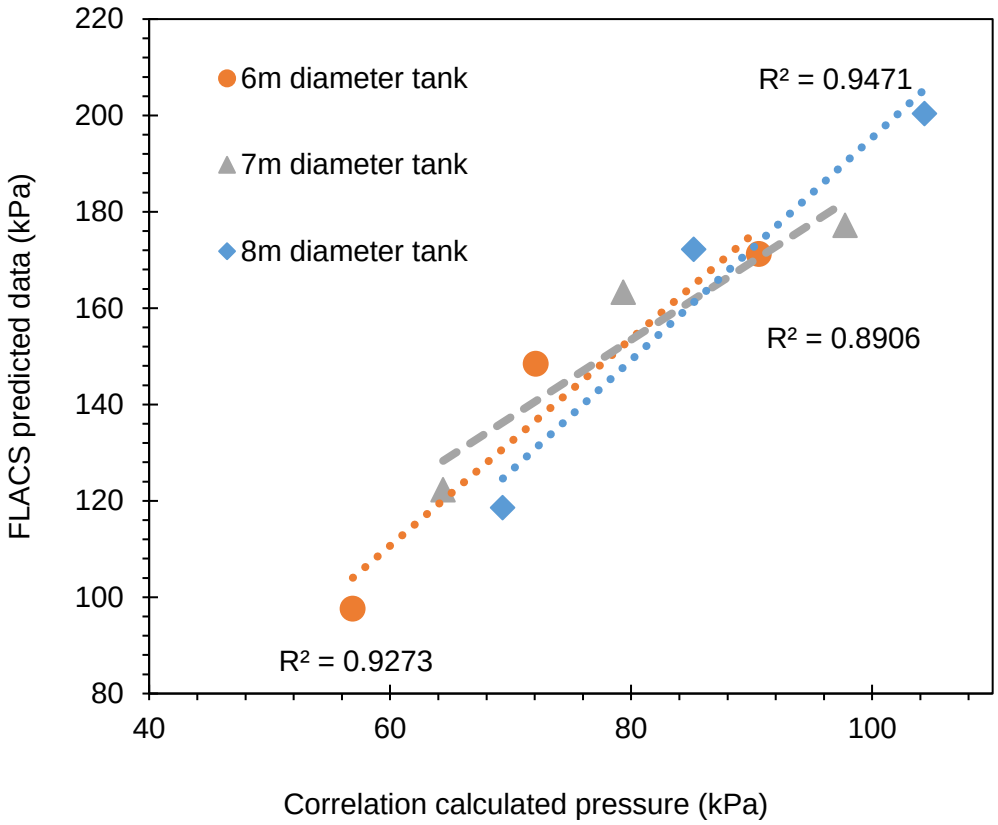

Fig. 22 Comparison of FLACS predicted pressures and correlation-calculated data

4. Parametric study

In section 3, the grid sensitivity study on large-scale twin tank explosion has been conducted. A series of FLACS simulations by using the chosen grid mesh have been carried out. It is proven that FLACS predicted pressures from these large-scale explosions are in good agreement with the data by using the analytical correlations with correct scaling. A more detailed parametric study is performed in this section to investigate the effect of separation distance between adjacent tanks on pressure and impulse mitigation by using these large-scale twin tanks. The interaction between the separation distance and various tank parameters is discussed.

4.1 Effect of separation distance on pressure and impulse from explosions of tanks of different diameters

To investigate the effect of separation distance on vented gas explosion mitigation, pressure and impulse data recorded from the pressure-accepting tanks are used. Meanwhile, since the pressures and impulses are not strictly uniform on a curved tank wall surface, an inactive/passive panel (as seen in Fig. 20) is used to average all data.

The tanks with diameter of 6m, 7m and 8m are firstly used for the investigation of the effect of separation distance on mitigation of pressure and impulse from vented explosions of tanks with different diameters. The diameters of pressure donor tank (tank filled with gas cloud) and pressure-accepting tank vary simultaneously from 6m to 8m. The tank height is fixed at 4m, vent area is 0.6m^2, and the separation gap is in the range of 1m to 3m.

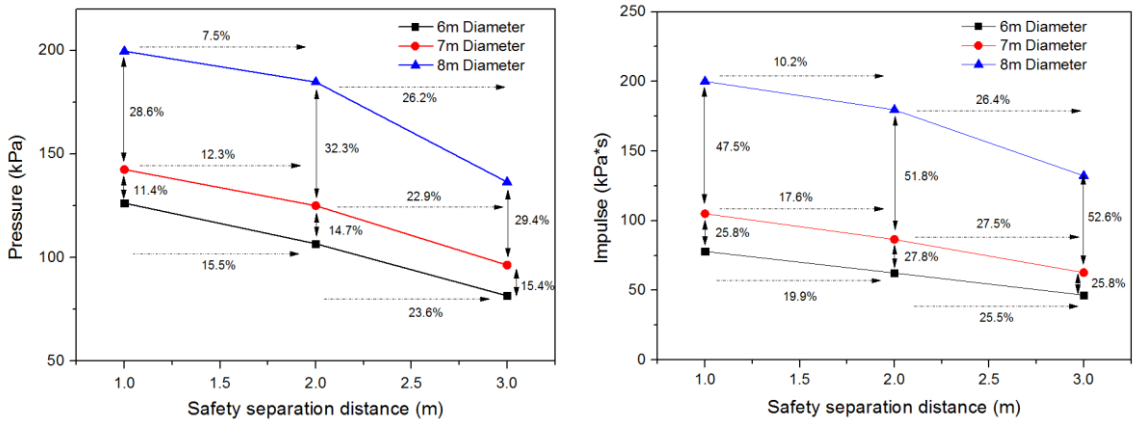

(a) Overpressure peak data **(b) Maximum impulse data**

Fig. 23 Pressure and impulse data from pressure-accepting tanks with 3 different diameters and 3 different separation distances

The overpressure peaks and maximum impulses from these 9 cases are extracted and shown in Fig. 23. The dashed horizontal arrows represent the level of pressure decrease when the separation distance increases 1m. The solid vertical arrows are the pressure differences between two different tank diameter cases. From the dashed horizontal arrows, it is seen that the pressure mitigation level is higher when the separation distance is bigger. For instance, the mitigation percentages are 26.2%, 22.9% and 23.6% (corresponding to 8m, 7m, and 6m diameter tanks) when the separation distance increases from 2m to 3m, whereas they are only 7.5%, 12.3 and 15.5% when the separation distance increases from 1m to 2m (Fig. 23(b)). The similar decaying

tendencies are seen in the impulse data of Fig. 23(b). In other words, the effect of increasing the separation distance on pressure and impulse mitigation is more obvious when the distance is large.

In terms of the solid vertical arrows, it is observed that the pressure and impulse decrease level (about 30% decrease and 50% decrease for pressure and impulse, respectively) are much more significant if the tank diameter reduces from 8m to 7m, while the pressure and impulse show about 14% and 26% decrease when the tank diameter shrinks from 7m to 6m. In other words, the decays in pressure and impulse are nonlinearly related to the reduction in tank diameter from the vented gas explosions.

In order to thoroughly investigate the tank diameter effect on external pressure and impulse, tank diameters ranging from 5.5m to 8.0m (6 different explosion cases) are considered. The separation distance is fixed as 1m and the results are shown in Fig. 24.

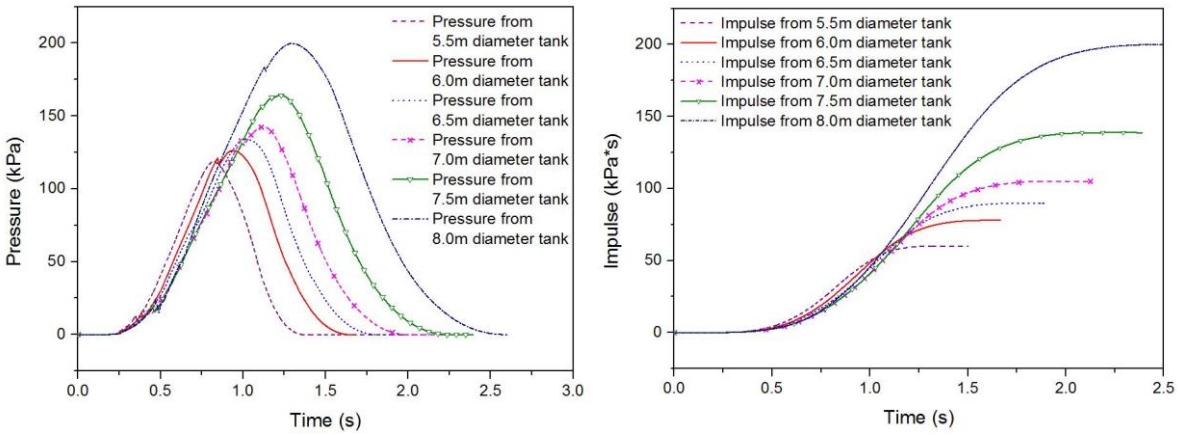

(a) Pressure-time history **(b) Impulse-time history**

Fig. 24 Pressure and impulse on the pressure-accepting tanks with different diameters

It is shown in Fig. 24 that by increasing the tank diameter from 5.5m to 8.0m, the overpressure peaks increase monotonically (Fig. 24(a)). The duration of pressure-time curve also increases, which is due to the longer combustion time inside the larger tank. It is known that impulse is the integral of pressure-time history. As both the overpressure peak and combustion time increase, the impulse increases more prominently than overpressure peak. Fig. 25 well

demonstrates the above observations. The maximum impulse versus tank diameter relationship curve has a more rapid increment rate than the overpressure peak curve.

The relationships among tank diameter, overpressure peak and impulse in Fig. 25 are expressed by two exponential growing curves, indicating both the pressure and impulse increase with the tank diameter exponentially.

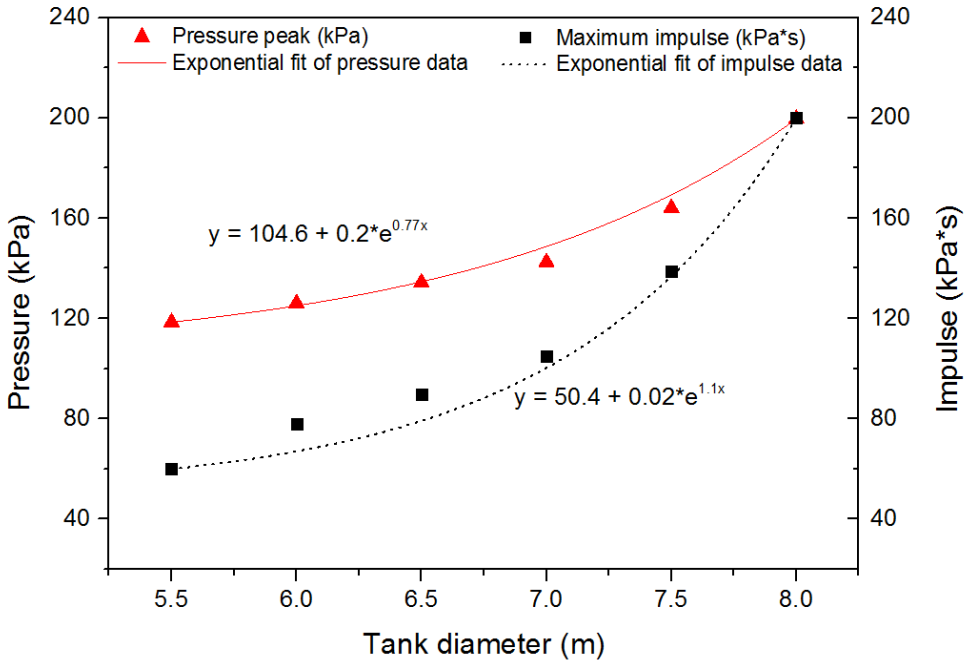

Fig. 25 Relationships among tank diameter, overpressure peak and maximum impulse

4.2 Effect of separation distance on explosion pressure and impulse from tanks of different vent area sizes

The separation distance effect on explosion pressure and impulse from tanks with different vent area sizes is investigated in this section. The 7m diameter and 4m height tank, which is the tank in the middle range of all tanks in section 4.1, is chosen for the study. The vent arrangement is the same as shown in Fig. 14. In the parametric study, vent area sizes of 0.6m^2, 0.8m^2 and 1.0m^2 are considered.

As seen in Fig. 26 (the dashed horizontal arrows), increasing the separation distance between tanks from 1m to 3m results in overpressure peak decrease for all vent area cases. Similar to

675 those observed in section 4.2, the pressure shows a larger reduction rate when the separation
676 distance is larger. The reason is that the pressure decays more severely when pressure wave
677 propagates in open space. Larger separation distance leads to more pressure decay and more
678 energy dissipation in the air.

679 Although it is well known that larger vent area results in smaller vented explosion pressure,
680 from the solid vertical arrows, it is interesting to see that increasing the vent area from 0.6m^2
681 to 0.8m^2, the pressure decreases 19.0% for the 1m separation case, while the pressure decreases
682 11.3% when the separation distance between adjacent tanks is 3m. Similarly, increasing the
683 vent area from 0.8m^2 to 1.0m^2, the pressure decreases 22.5% in the 1 m separation case,
684 whereas the pressure decreases 15.4% in the case with separation gap of 3m. These results
685 indicate the pressure decrease ratio is inversely proportional to the separation distance. In other
686 words, if the separation distance is larger, the pressure decrease less with the same increase in
687 vent area.

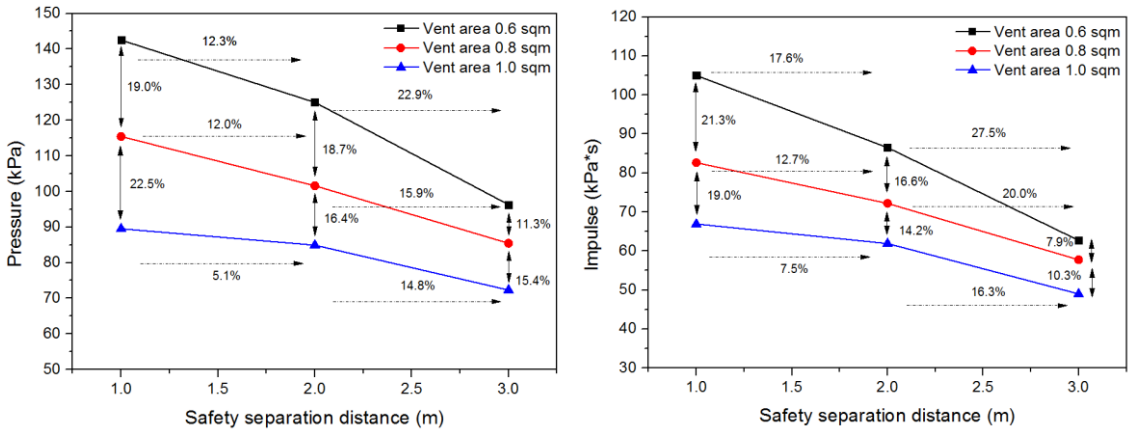

688
689 **(a) Peak pressure** **(b) Maximum impulse**
690 **Fig. 26 Pressure and impulse data from pressure-accepting tanks with 3 different vent areas and**
691 **3 different separation distances**
692
693 Similar observations regarding the effect of separation distance on explosion impulse as shown
694 in Fig. 26(b) can be drawn. As shown the impulse lines are even closer to each other on the
695 right hand side of the figure. It is known that changing the vent area is an effective way to
696 mitigate pressure and impulse. These results indicate that when the separation distance is large,

vent area effect on pressure and impulse mitigation becomes less prominent. Therefore, beside increasing the vent area, providing a large separation distance is also effective on pressure and impulse mitigation. When the separation distance is sufficiently large, increasing the vent area becomes less effective in mitigating the pressure and impulse.

4.3 Separation distance effect on explosion pressure and impulse for tanks of different heights

In this section, the separation distance effect on pressure and impulse mitigation is examined for tanks with different heights. The tank diameter is kept as 7m, vent area size is 0.6m^2. Separation distances considered are 1m, 2m and 3m. Tank heights are 4m, 6m and 8m. In total, 9 cases are simulated.

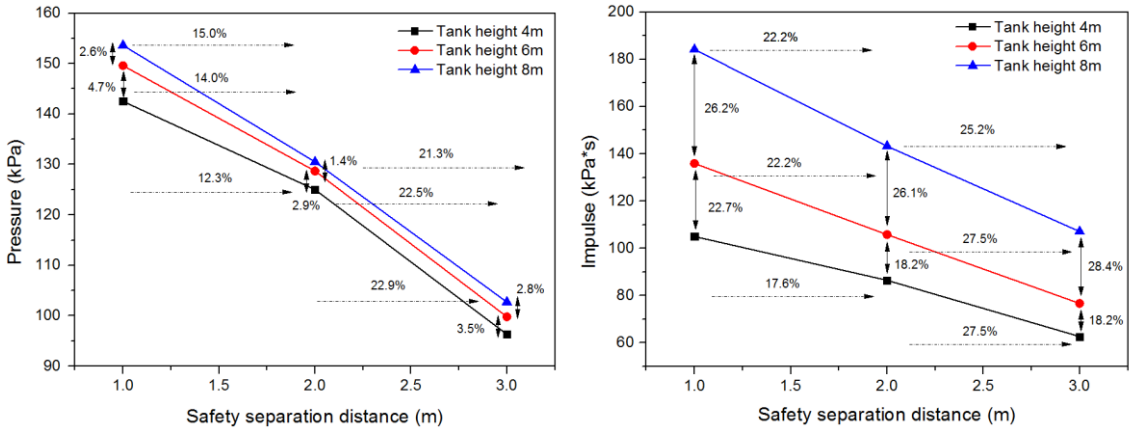

(a) Peak pressure **(b) Maximum impulse**

Fig. 27 Peak pressure and impulse from pressure-accepting tanks of 3 different heights and 3 different separation distances

Fig. 27 shows the peak pressure and impulse with respect to the different separation distances from tanks of three different heights. As shown at least 12.3% and 17.6% pressure and impulse reduction by increasing the separation distance from 1m to 2m can be achieved. The corresponding mitigation levels increase to 17.8% and 25.2% if the separation distance is increased from 2m to 3m. It is again proven that providing large separation distance is effective for mitigating pressure and impulse from vented explosions in adjacent tanks.

As shown in the figure (the solid vertical arrows), the differences in peak pressures from tanks of different heights are considerably smaller (between 1.4% and 4.7%) than the corresponding differences shown in Fig. 23 and Fig. 26, indicating tank diameter and vent area size are more influential parameters than tank height on explosion pressure. However, in Fig. 27(b), the differences between two vertical data are over 18.2%, which means reducing tank height is more effective in impulse mitigation than pressure reduction. Fig. 28 demonstrates the observations on tank height effect on pressure and impulse more thoroughly. As can be seen, overpressure peaks are marginally increased from explosions in the 4m height tank to the 8m height tank, while the maximum impulses are significantly increased. The reason is that the impulse is the integral of pressure over time, since the combustion duration is increased by extending the tank height, the final impulse value is therefore considerably increased as well.

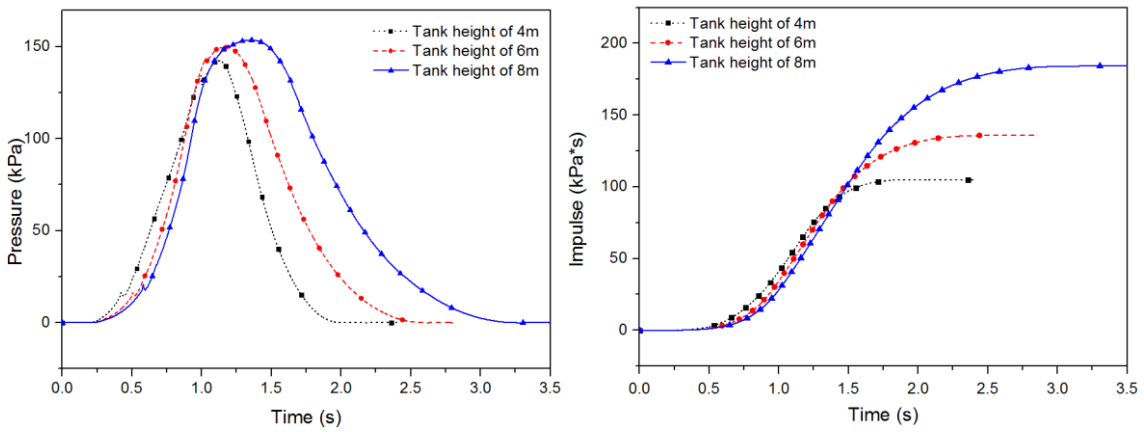

(a) Pressure-time history **(b) Impulse-time history**

Fig. 28 Pressure and impulse data for 3 different tank height cases with 1m separation distance

Therefore, according to the parametric studies of the effect of separation distances on mitigation of large-scale explosion pressure and impulse, it can be concluded that providing a large separation distance is very effective on pressure and impulse mitigation from adjacent tank explosions. When the separation distance is large, application of vent on explosion mitigation become less effective. Compared to the other two parameters, tank diameter is a more influential parameter than tank height on peak pressures recorded on adjacent tank wall.

741 However, reducing the tank height for a vented explosion can lead to significant reduction in
742 pressure impulse on adjacent tank wall although its effect on mitigating the peak pressure is
743 insignificant.

744

745 **5. Conclusion**

746 In this study, numerical and analytical study of vented gas explosion between large-scale twin
747 tanks is conducted. The large-scale explosion simulations are carried out by using CFD
748 software FLACS. Experimental data are used for the validation of FLACS simulation accuracy.
749 The FLACS predicted data agree well with all experimental results in this study. Sensitivity
750 study for the selection of correct meshing grids is performed for the large-scale models.

751 In the analytical study, the internal pressure and external pressure from vented gas explosion
752 in a cylindrical tank are investigated. It is proven in this study the authors' previously proposed
753 correlations are applicable for large-scale vented gas explosion overpressure peak prediction.
754 However, two scale-up factors are required for the adjustment of correlations.

755 According to the parametric study results, providing separation between tanks is effective on
756 reducing the pressure and impulse on adjacent tanks. The effectiveness of vent on explosion
757 mitigation is weakened when the separation distance is large. The larger diameter is the tank,
758 the higher are the explosion pressure and impulse. The peak pressure and impulse increase
759 exponentially with the tank diameter. Reducing tank height is effective in reducing the impulse
760 but has insignificant effect on the peak pressure acting on adjacent tanks.

761 **Acknowledgement**

762 The authors acknowledge partial financial supports from Australian Research Council project
763 (No. LP130100919) and China National 973 project (No. 2015CB058003) for carrying out this
764 research.

References

API-650. 2007. Welded Steel Tanks for Oil Strorage. *American Petroleum Institute, 11th Edition*.

Arntzen, B.J., 1998. Modelling of turbulence and combustion for simulation of gas explosions in complex geometries. Thesis. The Norwegian University

Bao, Q., Fang, Q., Zhang, Y.D., Chen, L., Yang, S.G., Li, Z., 2016. Effects of gas concentration and venting pressure on overpressure transients during vented explosion of methane-air mixtures. *Fuel*. 175, 40-48.

Bauwens, C.R., Chaffee, J., Dorofeev, S., 2010. Effect of Ignition Location, Vent Size, and Obstacles on Vented Explosion Overpressures in Propane-Air Mixtures. *Combust Sci Technol*. 182 (11-12), 1915-32.

Bauwens, C.R., Chao, J., Dorofeev, S.B., 2012. Effect of hydrogen concentration on vented explosion overpressures from lean hydrogen-air deflagrations. *Int J Hydrogen Energ*. 37 (22), 17599-605.

Bjerketvedt, D., Bakke, J.R., Van Wingerden, K., 1997. Gas explosion handbook. *J Hazard Mater*. 52 (1), 1-150.

Bradley, D., Mitcheson, A., 1978. The venting of gaseous explosions in spherical vessels. II—Theory and experiment. *Combustion and Flame*. 32, 237-55.

Cammarota, F., Di Benedetto, A., Russo, P., Salzano, E., 2010. Experimental analysis of gas explosions at non-atmospheric initial conditions in cylindrical vessel. *Process Safety and Environmental Protection*. 88 (5), 341-49.

Catlin, C.A., 1991. Scale Effects on the External Combustion Caused by Venting of a Confined Explosion. *Combustion and Flame*. 83 (3-4), 399-411.

Cen, K., Song, B., Huang, Y., Wang, Q.S., 2017. CFD Simulations to Study Parameters Affecting Gas Explosion Venting in Compressor Compartments. *Math Probl Eng*.

Ferrara, G., Di Benedetto, A., Salzano, E., Russo, G., 2006. CFD analysis of gas explosions vented through relief pipes. *J Hazard Mater*. 137 (2), 654-65.

Ferrara, G., Willacy, S.K., Phylaktou, H.N., Andrews, G.E., Di Benedetto, A., Salzano, E., Russo, G., 2008. Venting of gas explosion through relief ducts: Interaction between internal and external explosions. *J Hazard Mater*. 155 (1-2), 358-68.

Gexcon. 2017. FLACS v10.7 User's Manual, Norway.

Hansen, O.R., Hinze, P., Engel, D., Davis, S., 2010. Using computational fluid dynamics (CFD) for blast wave predictions. *J Loss Prevent Proc*. 23 (6), 885-906.

Hansen, O.R., Johnson, D.M., 2015. Improved far-field blast predictions from fast deflagrations, DDTs and detonations of vapour clouds using FLACS CFD. *J Loss Prevent Proc*. 35, 293-306.

Harrison, A.J., Eyre, J.A., 1987. External Explosions as a Result of Explosion Venting. *Combust Sci Technol*. 52 (1-3), 91-106.

Hisken, H., 2018. Investigation of instability and turbulence effects on gas explosions: experiments and modelling (Thesis). University of Bergen.

Hjertager, B.H., 1984. Computer-Simulation of Turbulent Reactive Gas-Dynamics. *Model Ident Control*. 5 (4), 211-36.

Hjertager, B.H., 1993. Computer Modeling of Turbulent Gas-Explosions in Complex 2d and 3d Geometries. *J Hazard Mater*. 34 (2), 173-97.

Kasmani, R.M., Ancirews, G.E., Phylaktou, H.N., 2013. Experimental study on vented gas explosion in a cylindrical vessel with a vent duct. *Process Safety and Environmental Protection*. 91 (4), 245-52.

Li, J., Hao, H., 2018. Far-field pressure prediction of a vented gas explosion from storage tanks by using new CFD simulation guidance. *Process Safety and Environmental Protection*. 119, 360-78.
Li, J., Hao, H., Shi, Y.C., Fang, Q., Li, Z., Chen, L., 2018. Experimental and computational Fluid Dynamics study of separation gap effect on gas explosion mitigation for methane storage tanks. *J Loss Prevent Proc*. 55, 359-80.
Li, J., Hernandez, F., Hao, H., Fang, Q., Xiang, H.B., Li, Z., Zhang, X., Chen, L., 2017. Vented Methane-air Explosion Overpressure Calculation—A simplified approach based on CFD. *Process Safety and Environmental Protection*. 109, 489-508.
Liu, Q.M., Zhang, Y.M., Niu, F., Li, L., 2015. Study on the flame propagation and gas explosion in propane/air mixtures. *Fuel*. 140, 677-84.
Mercx, W.P.M., Vanwingerden, C.J.M., Pasman, H.J., 1992. Venting of Gaseous Explosions. *Inst Chem E*. 130, 411-26.
Molkov, V., Dobashi, R., Suzuki, M., Hirano, T., 2000. Venting of deflagrations: hydrocarbon-air and hydrogen-air systems. *J Loss Prevent Proc*. 13 (3-5), 397-409.
Molkov, V., Kashkarov, S., 2015. Blast wave from a high-pressure gas tank rupture in a fire: Stand-alone and under-vehicle hydrogen tanks. *Int J Hydrogen Energ*. 40 (36), 12581-603.
NFPA-68. 2007. *Standard on explosion protection by deflagration venting* (National Fire Protection Association).
Nishimura, I., Mogi, T., Dobashi, R., 2013. Simple method for predicting pressure behavior during gas explosions in confined spaces considering flame instabilities. *J Loss Prevent Proc*. 26 (2), 351-54.
Pasman, H.J., 2015. *Risk Analysis and Control for Industrial Processes-Gas, Oil and Chemicals: A System Perspective for Assessing and Avoiding Low-Probability, High-Consequence Events* (Butterworth-Heinemann).
Pedersen, H.H., Middha, P., 2012. Modelling of Vented Gas Explosions in the CFD tool FLACS. *Chem Engineer Trans*. 26, 357-62.
REMBE. 2015. Explosion Safety Product Information. http://www.rembe.com/fileadmin/produkte/explosionsschutz/EGV/Product_Information_EGV.pdf.
Rodgers, S.A., Zalosh, R., 2013. NFPA 68 - New Gas Venting Equations. *AIChE* 9th Global congress on process safety.
Rota, R., Canu, P., Carra, S., Morbidelli, M., 1991. Vented Gas Deflagration Modeling - a Simplified Approach. *Combustion and Flame*. 85 (3-4), 319-30.
Russo, P., Di Benedetto, A., 2007. Effects of a duct on the venting of explosions - Critical review. *Process Safety and Environmental Protection*. 85 (B1), 9-22.
Solberg, D., Pappas, J., Skramstad, E., 1981. Observations of flame instabilities in large scale vented gas explosions. In *Symposium (International) on Combustion*. 1607-14. Elsevier.
Swift, I., 1989. Nfpa-68 Guide for Venting of Deflagrations - Whats New and How It Affects You. *J Loss Prevent Proc*. 2 (1), 5-15.
Tolias, I., Giannissi, S., Venetsanos, A., Keenan, J., Shentsov, V., Makarov, D., Coldrick, S., Kotchourko, A., Ren, K., Jedicke, O., 2018. Best practice guidelines in numerical simulations and CFD benchmarking for hydrogen safety applications. *Int J Hydrogen Energ*.
Tomlin, G., Johnson, D.M., Cronin, P., Phylaktou, H.N., Andrews, G.E., 2015. The effect of vent size and congestion in large-scale vented natural gas/air explosions. *J Loss Prevent Proc*. 35, 169-81.

Tsuruda, T., Hirano, T., 1987. Growth of Flame Front Turbulence during Flame Propagation across an Obstacle. *Combust Sci Technol*. 51 (4-6), 323-28.

Vyazmina, E., Jallais, S., 2016. Validation and recommendations for FLACS CFD and engineering approaches to model hydrogen vented explosions: Effects of concentration, obstruction vent area and ignition position. *Int J Hydrogen Energ*. 41 (33), 15101-09.

Vyazmina, E., Jallais, S., Krumenacker, L., Tripathi, A., Mahon, A., Commanay, J., Kudriakov, S., Studer, E., Vuillez, T., Rosset, F., 2018. Vented explosion of hydrogen/air mixture: An intercomparison benchmark exercise. *Int J Hydrogen Energ*.